

1 EC3 design of web-post buckling resistance for perforated steel beams with
2 elliptically-based web openings

3
4 Felipe Piana Vendramell Ferreira^{a*}, Rabee Shamass^b, Luis Fernando Pinho Santos^b, Vireen
5 Limbachiya^b, Konstantinos Daniel Tsavdaridis^c

6 ^aFederal University of Uberlândia, Faculty of Civil Engineering – Campus Santa Mônica, Uberlândia,
7 Minas Gerais, Brazil

8 ^bLondon South Bank University, School of Built Environment and Architecture, London, UK

9 ^cDepartment of Civil Engineering, School of Mathematics, Computer Science and Engineering, City,
10 University of London, Northampton Square, EC1V 0HB, London UK

11 *Corresponding author

12 **Abstract**

13 In this paper, the influence of the web-post geometric parameters on the shear buckling resistance of
14 perforated steel beams with previously proposed novel non-standard elliptically-based web openings is
15 investigated. An economical and practical approach to estimate the web-post buckling resistance in
16 accordance with EUROCODE 3 and the buckling resistance of the strut model analogy is developed and
17 analysed. Finite element models are developed and validated against test results available in the
18 literature. An extensive parametric study using Python code is carried out. A total of 5,400 geometrical
19 models is investigated and the analysed parameters are discussed in relation to the buckling curves. It is
20 concluded that the proposed design method for the web-post buckling resistance provides accurate and
21 reliable predictions and can be used for practical design purposes of perforated steel beams with
22 elliptically-based web openings.

23 **Keywords:** Steel beams; Elliptical web openings; Web-post buckling; Strut model; Eurocode 3.

24 E-mail addresses:

25 fpvferreira@ufu.br (F. P. V. Ferreira)

26 shamassr@lsbu.ac.uk (R. Shamass)

27 pinhosl3@lsbu.ac.uk (L. F. P. Santos)

28 limbachv@lsbu.ac.uk (V. Limbachiya)

29 konstantinos.tsavdaridis@city.ac.uk (K. D. Tsavdaridis)

30 **Notation**

31 The following symbols are used in this paper:

b_f	the flange width;	K	Coefficient in Eq. (19);
d	the parent section height;	l_{eff}	the web-post effective length;
d_g	the total height after castellation process;	R	the opening radius;
d_o	the opening height;	s	the web-post width;
d_t	the tee height;	t_f	the flange thickness;
$f_{cr,w}$	the critical shear stress in the web-post;	t_w	the web thickness;
f_y	the yield strength of the steel section;	V	the global shear;
f_u	the ultimate stress of the steel section;	w	the opening width;
h	the distance between flanges geometric centres of the parent section;	ε	strain;
H	the distance between flanges geometric centres after castellation process;	λ_o	the reduced slenderness factor;
k	Coefficient in Eq. (10);	λ_w	the web-post slenderness factor;
		σ	stress;
		χ	the reduction factor;

32

33 **1. INTRODUCTION**

34 Perforated steel beams with periodical web openings are manufactured using the
35 castellation process (aka profile cutting procedure), which consists of three steps:
36 thermal cutting of the initial (parent) section, separation of the two halves, and welding.
37 The result of this process is an expanded (deeper) section. The steel beams with
38 periodical web openings are classified based on the shape of the web opening. The
39 castellated, cellular and AngelinasTM [1] beams are those with hexagonal, circular and
40 sinusoidal web openings, respectively. These steel beams have been used in
41 construction, mainly due to many advantages such as greater flexural stiffness due
42 castellation process, self-weight reduction and structural floor height reduction as the

43 web openings allow the integration of hydraulic and electric services (instead of them
44 running under the steel beams).

45 The flexural behaviour of the perforated steel beams with periodical web openings
46 can be a complex problem as they are prone to several failure modes such as a
47 plasticisation mechanism, due to the Vierendeel bending, and buckling modes such as
48 lateral-torsional, web-post¹, web distortional or even the combination between them [2–
49 8]. The present study focuses on the web-post buckling failure which occurs for steel
50 beams with closely spaced periodical web openings that have thin-walled nature [9]. It
51 is a local phenomenon, in which the final configuration of the web-post is characterised
52 by a lateral displacement with torsion due to the horizontal shear at the web-post. The
53 main geometric parameters that influence the web-post buckling resistance are the
54 opening height, the web-post width, and the web thickness [10–13]. In the literature,
55 various research recommendations were suggested to predict the web-post buckling
56 resistance of perforated steel beams. For example, Fares et al. [13] published
57 recommendations and design guidance for cellular and castellated steel beam in
58 accordance with ANSI/AISC 360-16 [14]. Their design guidance is based on an early
59 empirical design method in Ward's work [15]. On the other hand, Lawson and Hicks
60 [16] suggested different design method to calculate the web-post buckling resistance of
61 cellular beams with and without elongated openings based on the design of compressed
62 diagonal strut and the compressive stress is calculated according to EC3 [17], while the
63 web-post buckling resistance of AngelinasTM can be obtained from the software ACB+
64 developed by Centre Technique Industriel de la Construction Métallique (CTICM) for
65 ArcelorMittal [1].

¹The AngelinasTM, although they present a buckling mode in the web-post, this mode is not characterised as a double curvature in an “S” shape, such as the web-post buckling of castellated and cellular beams.

66 Researchers sought to optimise the opening shape for a better distribution of
67 stresses, and consequently, the increase of resistance. In this context, the works of are
68 highlighted. Early works of Tsavdaridis and D’Mello [23] investigated the Vierendeel
69 bending and web-post buckling resistance of steel beams with various non-standard web
70 openings. It was highlighted that vertical elliptical (vertical major axis) web openings
71 presented positive results. In particular, the optimised novel elliptically-based web
72 openings provided smooth edges that resisted the formation of plastic hinges at low
73 values of load while the stress concentration is controlled and occurred at positions
74 nearer to the neutral axis – at the intersection of the semi-circle and the lines [10,23,24].
75 Perforated beams with non-standard web openings were patented (GB 2492176 [25]) by
76 the authors.

77 Specifically, in Tsavdaridis and D’Mello [10] tests were carried out on short span
78 steel beams with different web openings shapes (i.e. circular with and without fillets
79 and elliptically-based), considering three-point bending. In this study, the web-post
80 resistance was main failure to be investigated. Finite element models were validated
81 and parametric studies were conducted varying the ratios of web-post width to opening
82 height and opening height to web-thickness. The authors concluded that elliptically-
83 based web openings had shown better stress distribution and greater resistance to
84 horizontal shear stresses in comparisons with circular web openings. Also, the authors
85 proposed an equation to predict the web-post buckling resistance by global shear based
86 on parameters studied. Importantly, this equation is applied to $d/t_w=30-80.77$ and
87 $t_w=3.9-10.5\text{mm}$. Later, Tsavdaridis and D’Mello [24] conducted an optimisation study of
88 these elliptically-based web openings and their resistance to the Vierendeel mechanism.
89 In this work, which was based on the finite element method, the authors concluded that
90 the elliptical web openings presented an increase in the flexural stiffness. Consequently,

91 steel beams with elliptically-based web openings presented lower deflections when
92 compared to steel beams with web circular openings.

93 Limited investigation has been carried out on perforated steel beams with
94 elliptically-based web openings. For practical and design purposes, this paper aims to
95 investigate the web-post buckling resistance of steel beams with elliptically-based web
96 openings (**Fig. 1**), as it is the most critical failure mode for such kind of structural
97 members. The procedure is based on defining the effective length of diagonal strut
98 analogy in the web-post while the buckling resistance of the compressed struct is
99 calculated using EC3 [17]. As seen in the **Fig. 1**, b_f , t_f , t_w and d are the flange width and
100 thickness, web thickness and the height of the parent section, respectively, H is the
101 cellular beam height after castellation process, d_o , w and R are the opening height, width
102 and radius, respectively, and s and b_w are the opening spacing and web-post width,
103 respectively. For this task, a finite element models were developed and validated
104 against the tests data conducted by Tsavdaridis and D'Mello [10]. A parametric study
105 is carried out, considering buckling, post-buckling and geometrical nonlinear analyses.
106 The geometric parameters ratios d/H , d_o/H , R/d_o and w/d_o are varied with respect to the
107 castellation process. A total of 5,400 geometrical models is analysed. The numerical
108 results are used to developed an equation in line with EC3 [17]. In the next section, the
109 development of the finite element model is presented.

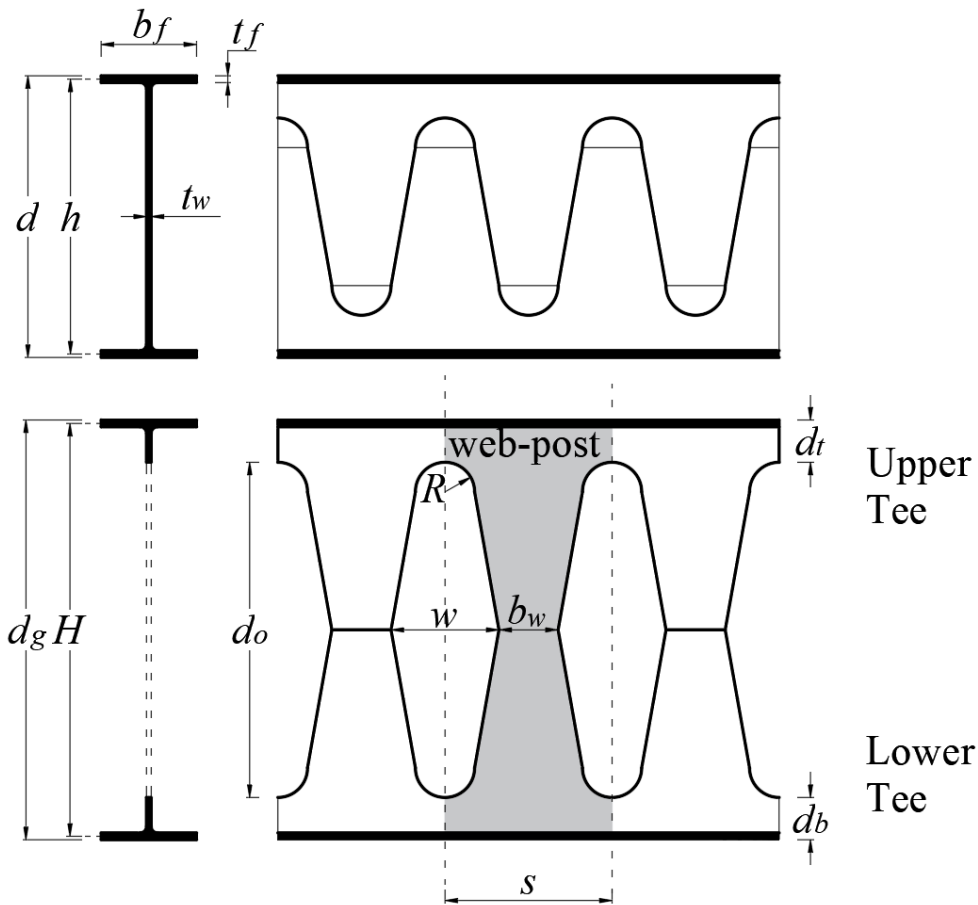


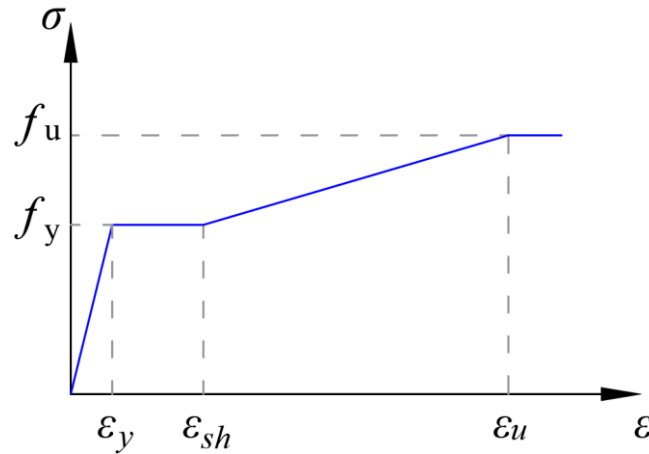
Fig. 1: Castellation process of steel beams with elliptically-based web openings [24]

2. FINITE ELEMENT ANALYSIS

The validation study is presented in two steps. Initially, the modelling is performed based on the experimental tests carried out in Tsavdaridis and D'Mello [11]. These models will be called here as full models. In the second part, single web-post models are developed. This approach has been widely used by researchers i.e. Zaarour and Redwood [25], Panedpojaman et al. [13], Tsavdaridis and Galiatsatos [26], Durif et al. [27], Grilo et al. [10], Limbachiya and Shamass [12], as it is possible to analyse separately the main parameters that influence the web-post buckling resistance, such as the web-post width and the opening height.

All models are processed in the ABAQUS software in two steps: buckling and post-buckling analyses. The geometrically and materially nonlinear analysis with

124 imperfections included (GMNIA) has been used by researchers of steel beams with
 125 periodical web openings, i.e. Ferreira et al. [28–33], Komal et al. [34], Ellobody [3,5],
 126 Panedpojaman et al [4] and Shamass and Guarracino [35]. The imperfection factor
 127 adopted was $d_g/500$. This factor was also used by Panedpojaman et al. [13], since the
 128 estimation of physical and geometric imperfections on steel beams with web openings is
 129 complex due to the manufacturing processes. Nominal strength values of the S355 steel
 130 are used². The modulus of elasticity and Poisson's coefficient are taken equal to 200GPa
 131 and 0.3, respectively. A multi-linear constitutive model (Fig. 2) is considered, similarly
 132 to the methodology applied in Shamass and Guarracino [35]. The values of ε_{sh} and ε_u
 133 were calculated as Yun and Gardner [36], according to the Eqs. (1-2). The stress- strain
 134 relationship implementation must be done with the real values (Eqs. 3-4).



135

136

Fig. 2: Multi-linear constitutive model for steel

$$\varepsilon_u = 0.6 \left(1 - \frac{f_y}{f_u} \right), \quad \varepsilon_u \geq 0.06 \quad (1)$$

$$\varepsilon_{sh} = 0.1 \frac{f_y}{f_u} - 0.055, \quad 0.015 < \varepsilon_{sh} \leq 0.03 \quad (2)$$

²According to tensile coupon tests performed by Tsavdaridis and D'Mello [11], the yield strength of the web and flange/stiffener were 375.3MPa and 359.7MPa, respectively, and the ultimate stresses were 492.7MPa and 480.9MPa for web and flange/stiffener, respectively. These values are close to the nominal strength values of S355.

$$\sigma^{true} = \sigma^{nom} (1 + \varepsilon^{nom}) \quad (3)$$

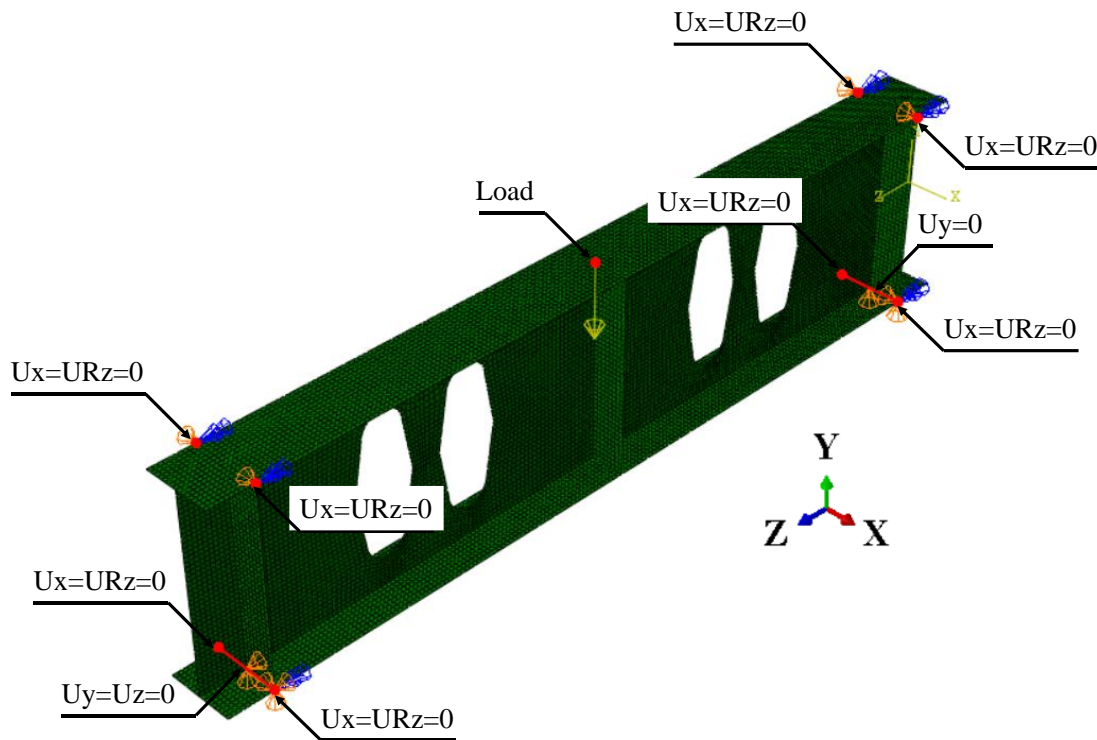
$$\varepsilon^{true} = \ln(1 + \varepsilon^{nom}) \quad (4)$$

137 Based on the mesh sensitivity analysis and recommendation by Ferreira et al.
 138 [31] and Ferreira and Martins [7], the element mesh size taken was 10 mm. The steel
 139 beam and stiffnesses were modelled using a general-purpose three-dimensional reduced
 140 integration shell element, named S4R. S4R has six degrees of freedom - three rotations
 141 and three translations that provide accurate results with less computational effort. The
 142 boundary conditions used for the full and single web-post models, as well as the
 143 validation results, are presented in the subsections below.

144

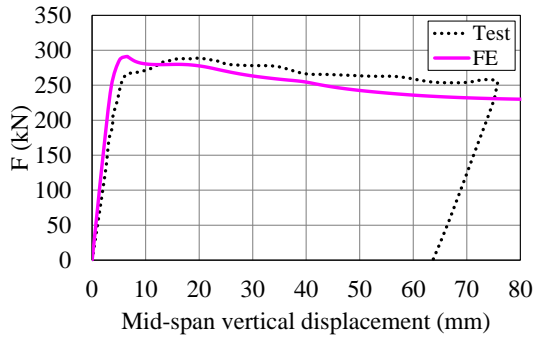
145 2.1 FULL MODELS

146 The experimental tests employed for the validation study are conducted by
 147 Tsavdaridis and D’Mello [11]. Specimens A1 and B1 are cellular beams with circular
 148 web openings opening, and specimen A2 is a cellular beam with fillets introduced at the
 149 mid-depth of the cellular web opening to ease their fabrication. B2 and B3 are perforated
 150 sections with the proposed novel vertical elliptically-based web openings. The boundary
 151 conditions of the full models are shown in **Fig. 3**. The analysis is performed with load
 152 control and the arc-length method is employed to capture the buckling behaviour. At
 153 the bottom of the stiffener in one end, vertical and longitudinal displacements are
 154 restrained ($U_y=U_z=0$). At the bottom of the stiffener in the other end, only the vertical
 155 displacement is restrained ($U_y=0$). At both ends, in the region of the stiffeners, lateral
 156 displacement and the rotation around the longitudinal axis are restrained at four points
 157 ($U_x=U_{Rz}=0$).

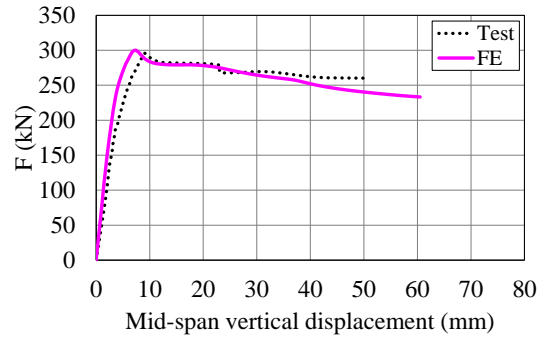


158
159 **Fig. 3: Boundary conditions of the full models, considering B3 model**

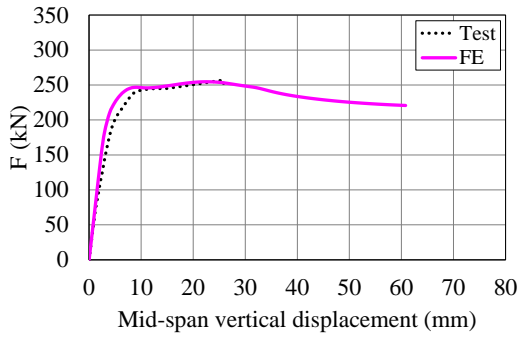
160 The validation results are presented by comparing the equilibrium trajectories of
161 both tests and full models, considering the load-deflection relationships (**Fig. 4**). As
162 shown in the models A1 (**Fig. 4a**), A2 (**Fig. 4b**), B1 (**Fig. 4c**), B2 (**Fig. 4d**) and B3 (**Fig.**
163 **4e**), the load-displacements relationships of numerical models are in agreement with
164 tests. The deformed beams tested by Tsavdaridis and D'Mello [11], are compared with
165 the results of the finite element method (**Fig. 5**). It is possible to notice that in all
166 analyses, considering the models A1 (**Fig. 5a**), A2 (**Fig. 5b**), B1 (**Fig. 5c**), B2 (**Fig. 5d**) and
167 B3 (**Fig. 5e**), the mode of failure was characterised by web-post buckling, similarly to
168 the tests. Furthermore, in **Table 1**, the values of the peak load of the tests and numerical
169 models are summarised. In view of the results presented so far, it is possible to conclude
170 that the numerical models are adequately validated, since the results showed a low
171 relative error in comparison to the tests.



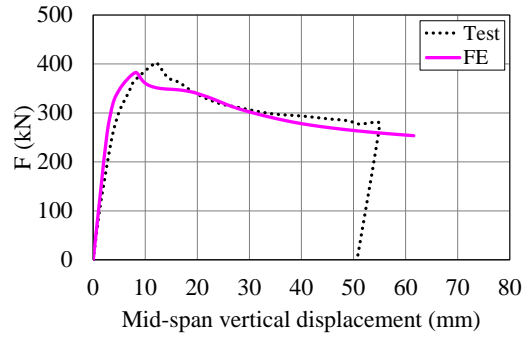
(a) A1



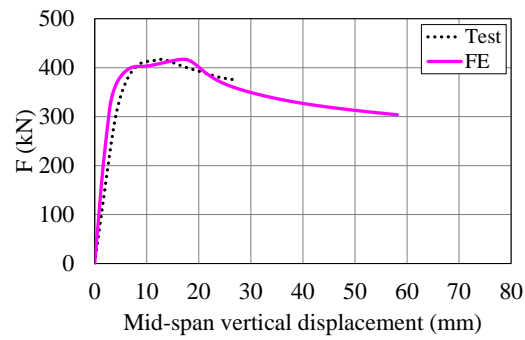
(b) A2



(c) B1



(d) B2



(e) B3

Fig. 4: Tests and finite element model by load-displacement relationships

172

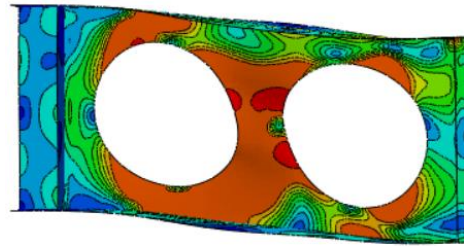
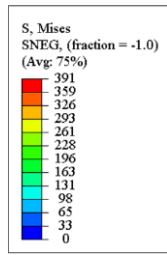
173

174

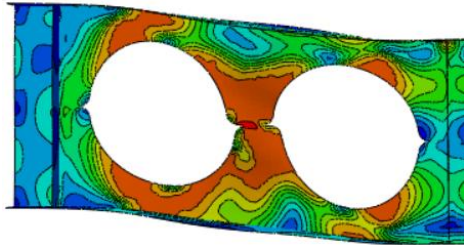
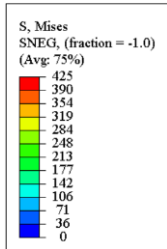
175

176

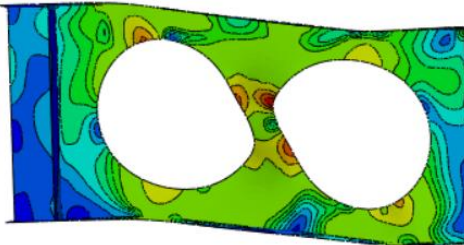
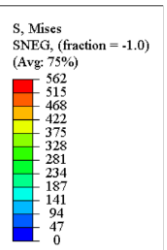
177



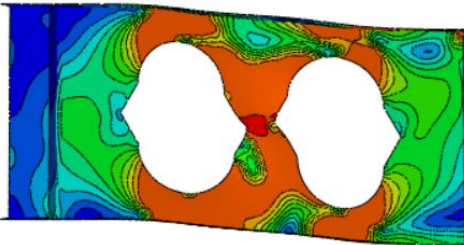
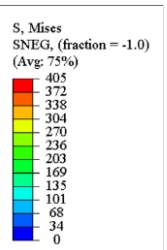
(a) A1



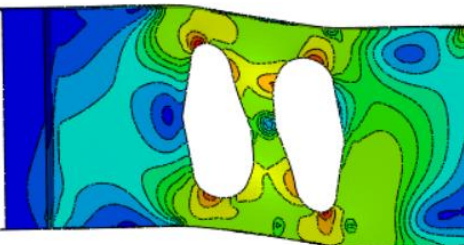
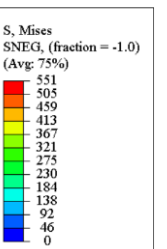
(b) A2



(c) B1



(d) B2



(e) B3

178 Fig. 5: Final configuration between tests performed by Tsavdaridis and D'Mello [11] with finite element
179 model

180

181 **Table 1: Summary of full models results**

Test	F_{Test} (kN)	F_{FE} (kN)	$(F_{FE}/F_{Test}-1)\%$	Failure
A1	288.7	291.0	0.8%	WPB
A2	298.0	300.0	0.7%	WPB
B1	255.0	254.5	-0.2%	WPB
B2	402.4	382.7	-4.9%	WPB
B3	415.0	417.1	0.5%	WPB

182

183 **2.2 SINGLE WEB-POST MODELS**

184 Single web-post models were also developed and validated to conduct parametric
185 studies. After several trials and comparisons with the test results, the boundary
186 conditions shown in in **Fig. 6** were used, leading to reasonably accurate predictions. On
187 one end, at both the flange and web of the tee sections, lateral, vertical and longitudinal
188 displacements are restrained ($U_x=U_y=U_z=0$). On the other end, lateral displacement as
189 well as rotations about the vertical and longitudinal axes are restrained
190 ($U_x=U_{Ry}=U_{Rz}=0$) at the flanges of both upper and lower tees. At that same end, lateral
191 displacement as well as rotations about to the lateral and vertical axes are restrained
192 at the webs of both upper and lower tees ($U_x=U_{Rx}=U_{Ry}=0$). Finally, the shell edge load
193 was applied along the web of the tee sections on the right hand side of the model, as
194 seen in the **Fig. 6**. The mesh size used in this model was of 3mm and 8mm for web and
195 flanges, respectively. In **Table 2**, the shear load results calculated from FE (V_{FE}) are
196 compared with those obtained from the tests (V_{Test}). It can be noted that the percentage
197 difference between FE and the test shear loads varies between 9.4% to -8.8% with an
198 average of -0.14% and coefficient of variation of 0.14%. Hence, the proposed web-post
199 model can be reasonably accurate and used for further parametric studies to predict the
200 shear load capacity of the web-post.

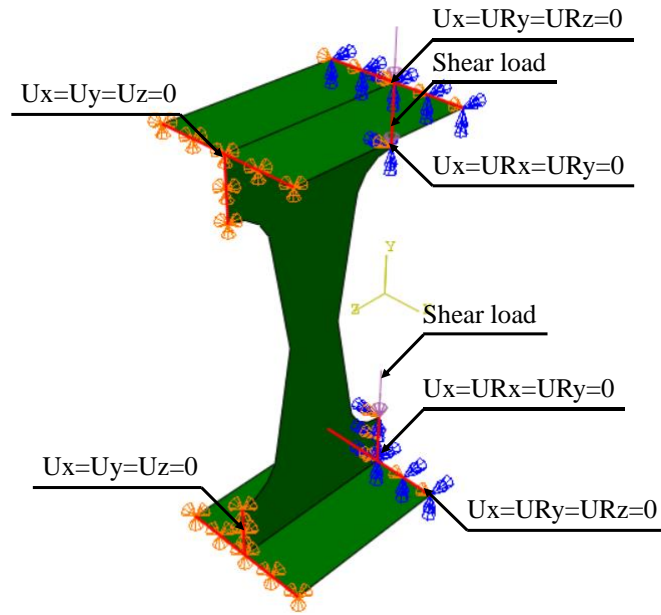


Fig. 6: Boundary conditions of the web-post models

Table 2: Summary of web-post models results

Test	V_{Test} (kN)	V_{FE} (kN)	Failure	$(V_{FE}/V_{Test}-1)\%$
A1	144.4	157.0	WPB	8.8%
A2	149.0	159.0	WPB	6.7%
B1	127.5	121.0	WPB	-5.1%
B2	201.2	200.5	WPB	-0.3%
B3	207.5	188.0	WPB	-9.4%
			S.D.	6.93%
			Var.	0.48%

2.3 PARAMETRIC STUDY

In total, twelve UB sections are considered (Table 3). For each UB section, the geometric ratios H/d , d/H , R/d_o and w/d_o are varied (Fig. 1) with respect to the castellation process (Eq. 5). The variations performed are:

- $H/d=1.2, 1.3, 1.4, 1.5$ and 1.6 ;
- $d/H=0.65, 0.70, 0.75, 0.80, 0.85$ and 0.90 ;
- $R/d_o=0.10, 0.15, 0.20, 0.25, 0.30, 0.35$ and 0.40 ;

212 • $w/d_o=0.25, 0.35, 0.45, 0.55$ and 0.65 .

$$H = 2h - 2d_t - 2R \quad (5)$$

213 **Table 3: UB sections**

UB Section	d (mm)	b_f (mm)	t_f (mm)	t_w (mm)
178x102x19	177.8	101.2	7.9	4.8
305x102x25	305.1	101.6	7.0	5.8
305x102x33	312.7	102.4	10.8	6.6
305x127x48	311.0	125.3	14.0	9.0
457x152x52	449.8	152.4	10.9	7.6
457x191x133	480.6	196.7	26.3	15.3
533x210x122	544.5	211.9	21.3	12.7
533x312x272	577.1	320.2	37.6	21.1
686x254x170	692.9	255.8	23.7	14.5
838x292x176	834.9	291.7	18.8	14.0
914x305x201	903.0	303.3	20.2	15.1
1016x305x487	1036.3	308.5	54.1	30.0

214 Each model of the parametric study is processed in two steps, (1) eigenvalue
 215 buckling analysis followed by (2) geometrical nonlinear analyses with imperfections. In
 216 addition, geometrical nonlinear analysis without imperfections is considered. The
 217 geometric nonlinear analysis with imperfections is performed with the objective of
 218 defining the web-post buckling mode and obtain the capacity resistance of the structural
 219 component. Python script is developed to conduct the parametric study as well as post-
 220 process the results.

221 The script can create the FE model for a given web geometry defined by the
 222 parameters in **Fig 1** and the boundary condition shown in **Fig.6**. The script firstly
 223 performed eigenvalue buckling analysis to define the lowest buckling mode that was
 224 used as initial imperfection shape while the imperfection size was $d_g/500$. Then, it

225 performed nonlinear analysis using a Newton-Raphson solution method in order to
 226 obtain the buckling load, while both the buckling load and the failure mode were stored
 227 for analysis. The script is publicly available at <https://github.com/luisantos090/WPB>.

228

229 3. RESULTS AND DISCUSSION

230 From the 5,400 geometrical models analysed, 4,344 models had the resistance
 231 defined by web-post buckling. The results are discussed, considering the influence of the
 232 parameters, as well the web-post buckling resistance according to EC3 buckling curves
 233 [18], which are presented in the Eq. (6-8).

$$\chi = \frac{1}{\phi + \sqrt{\phi^2 - \lambda_0^2}} \leq 1.0 \quad (6)$$

$$\phi = 0.5 \left[1 + 0.49(\lambda_0 - 0.2) + \lambda_0^2 \right] \quad (7)$$

$$\lambda_0 = \sqrt{\frac{f_y}{f_{cr,w}}} \quad (8)$$

234 **Table 4: Imperfection factors for buckling curves**

Buckling curve	<i>a</i>	<i>b</i>	<i>c</i>	<i>d</i>
Imperfection factor (<i>a</i>)	0.21	0.34	0.49	0.76

235 The results of elastic buckling (from the eigenvalue analysis), and post-buckling
 236 analyses (i.e., web-post buckling resistance) are normalised in accordance with the EC3
 237 buckling curves, considering the parent section and H/d , d/H , R/d_o and w/d_o ratios. A
 238 similar analysis was presented in Ferreira et al. [28], however, it considered steel-
 239 concrete composite cellular beam models and focused on web-post buckling resistance.
 240 It is important to highlight that SCI P355 [17] employed the strut analogy for
 241 calculating the web-post buckling resistance. In this model, the buckling compressive
 242 stress of the strut with an effective length, is calculated according to EC3, in a similar

243 way of calculating the plastic buckling of compression members. The choice of buckling
 244 curve is a function of the geometric parameters of the steel profile, such as the flange
 245 thickness and width and the cross section height. For cellular steel beams with
 246 periodical circular web openings, SCI P355 [17] recommends using the buckling curve
 247 b and the buckling curve c for hot-rolled and welded (plated) sections, respectively. It is
 248 important to note that due to the castellation process, steel beams with elliptically-
 249 based web openings undergo the welding process, according to **Fig. 1**, hence, buckling
 250 curve c was chosen.

251 To normalise the numerical results with the EC3 buckling curves, the critical
 252 ($f_{cr,w,FE}$) and ultimate ($\sigma_{u,FE}$) shear stresses acting in the web-post, which are predicted
 253 by the critical ($V_{cr,FE}$) and ultimate ($V_{u,FE}$) shear forces considering buckling and post-
 254 buckling analyses, respectively, and are calculated according to **Eqs. (9-10)**. The
 255 normalised results, which are obtained by using the nominal values of S355 steel, are
 256 shown in **Fig. 7**. The geometric parameters of the web-post of perforated steel beams
 257 with elliptically-based web openings were presented in **Fig. 1**.

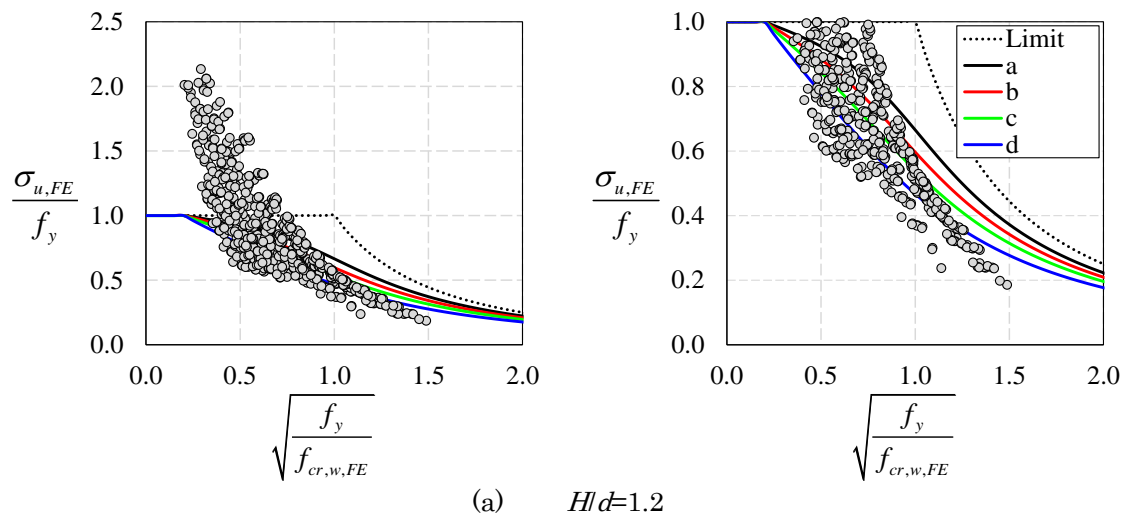
$$f_{cr,w,FE} = \frac{V_{cr,FE}}{t_w (s - w)} \quad (9)$$

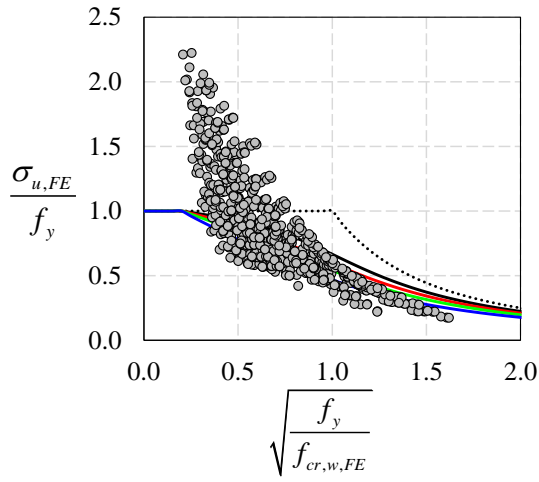
$$\sigma_{u,FE} = \frac{V_{u,FE}}{t_w (s - w)} \quad (10)$$

258 3.1 H/d ratio

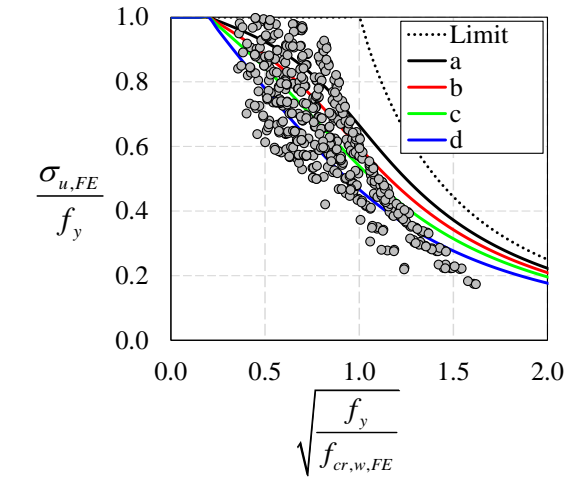
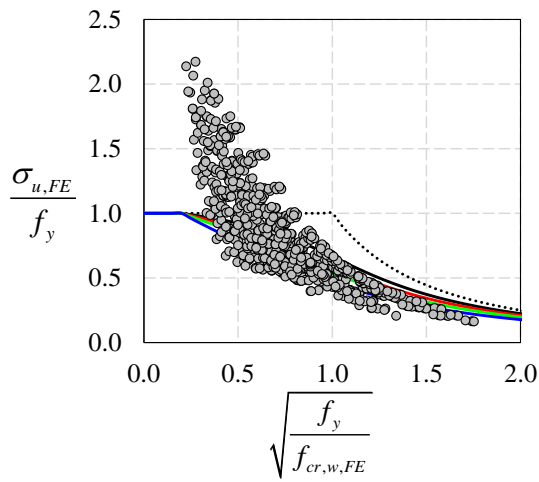
259 The H/d ratio refers to the expansion factor, that is, the ratio of the height of the
 260 section with the elliptically-based web opening to the parent section, according to **Fig.**
 261 **1. Fig. 7** shows the normalised results for the EC3 buckling curves, considering the
 262 expansion factor variation. Each series is presented in two figures. The first one shows
 263 the maximum values of resistance, and the second one is a zoom in of the first graph to

264 better show the results and the buckling curves. The expansion factors were $H/d=1.1$
 265 (Fig. 7a), $H/d=1.2$ (Fig. 7b), $H/d=1.3$ (Fig. 7c), $H/d=1.4$ (Fig. 7d), $H/d=1.5$ (Fig. 7e),
 266 $H/d=1.6$ (Fig. 7f), $H/d=1.7$ (Fig. 7g), $H/d=1.8$ (Fig. 7h) and $H/d=1.9$ (Fig. 7i). It was
 267 verified that the smaller the expansion factor, the smaller the web-post slenderness,
 268 and consequently, the smaller the effective length. This causes an increase in capacity
 269 resistance. However, the greater the reduced slenderness (λ_D), the lower the capacity
 270 resistance. It is important to highlight that although the results shown here illustrate
 271 the response as a function of the expansion factor (H/d) with respect to the castellation
 272 process, there were models that vary the other geometric parameters of the section with
 273 these elliptically-based web openings for the same expansion factor, such as the opening
 274 height, the web-post width and the opening radius. Once these parameters were varied,
 275 the effective length changes, and consequently, the web-post buckling resistance
 276 changes. The effective length will be presented in section 4 with more details.

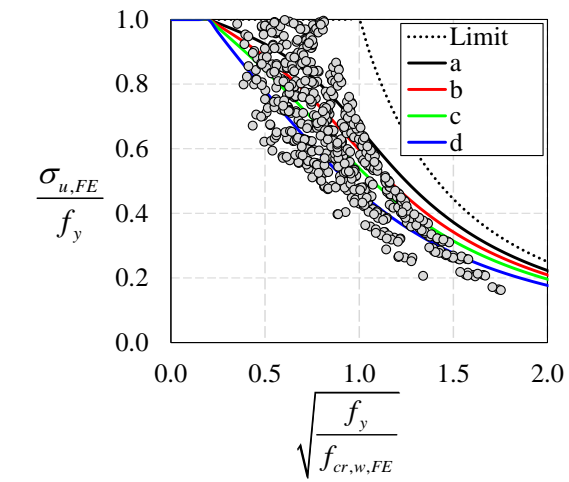
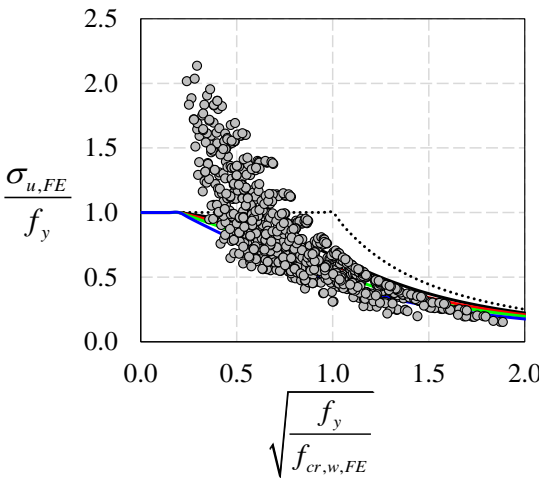




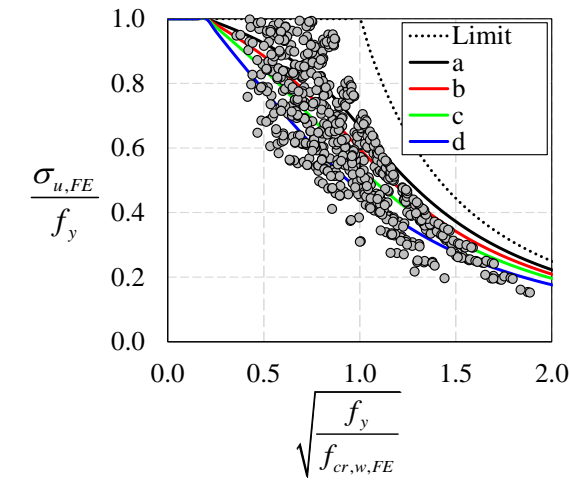
(b)

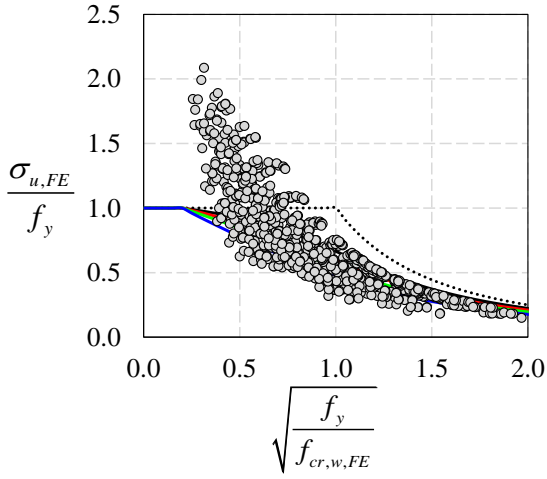
 $H/d=1.3$ 

(c)

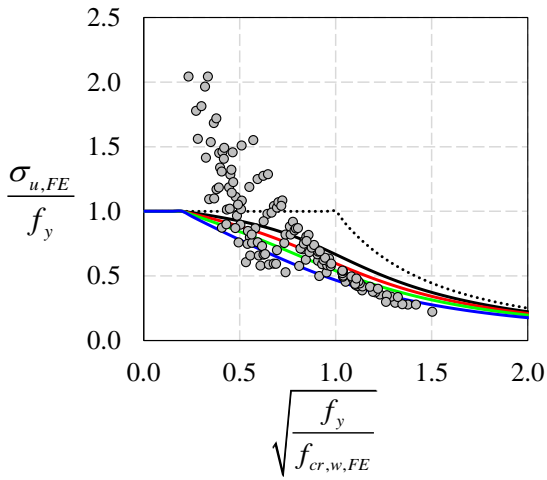
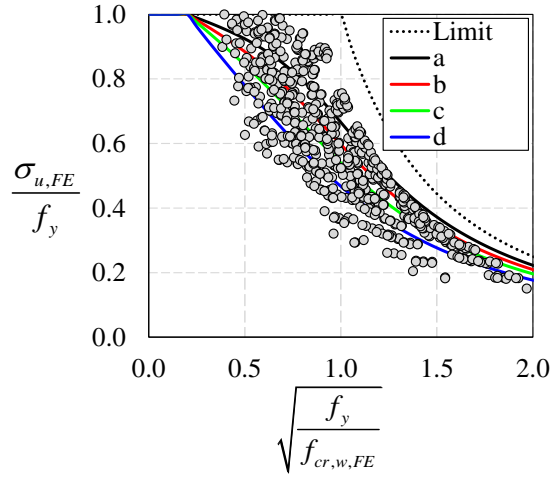
 $H/d=1.4$ 

(d)

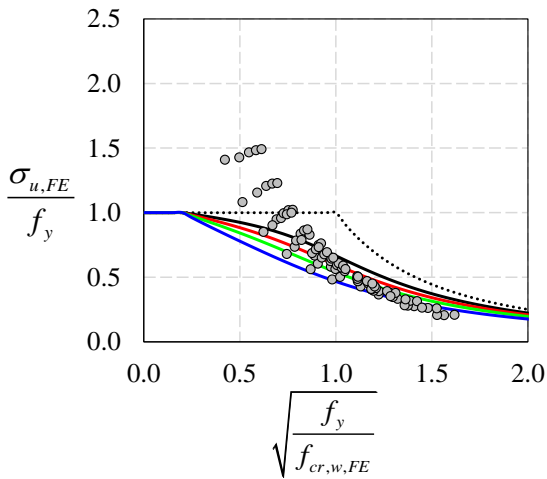
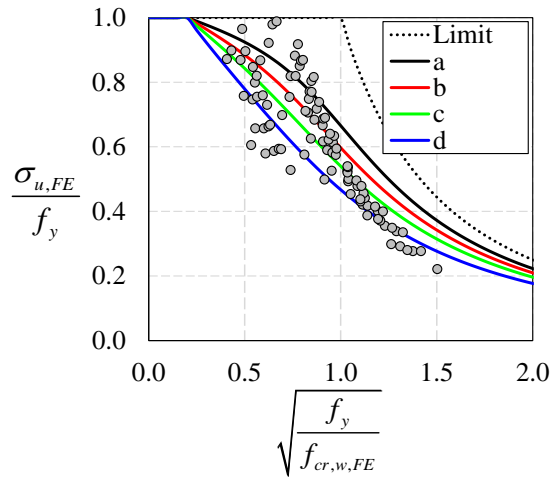
 $H/d=1.5$



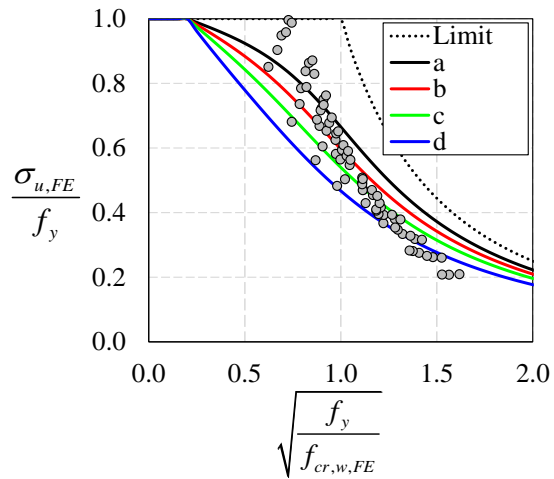
(e) $H/d=1.6$

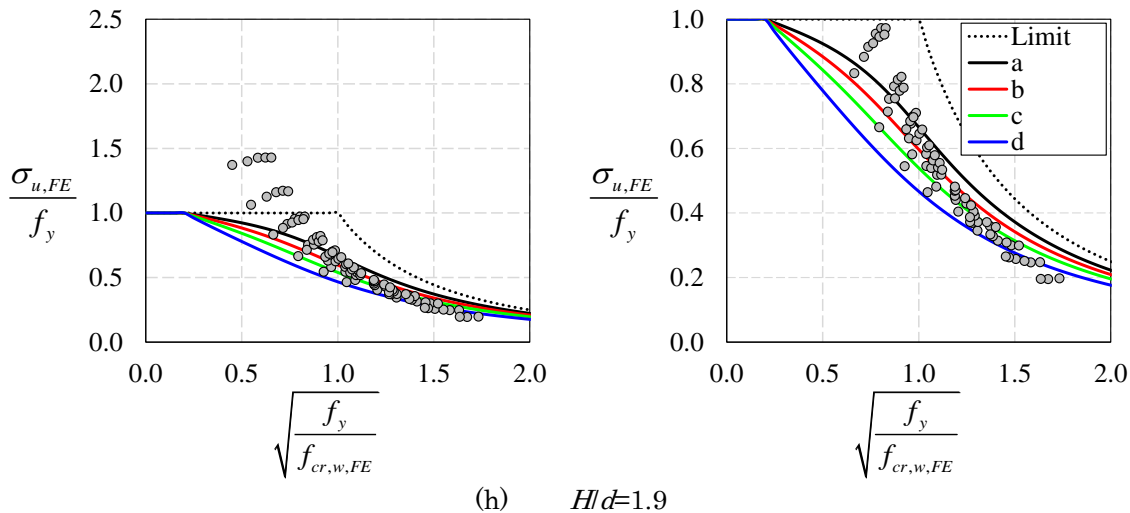


(f) $H/d=1.7$



(g) $H/d=1.8$





(h) $H/d=1.9$
Fig. 7: H/d ratio vs. buckling curves of EC3

277

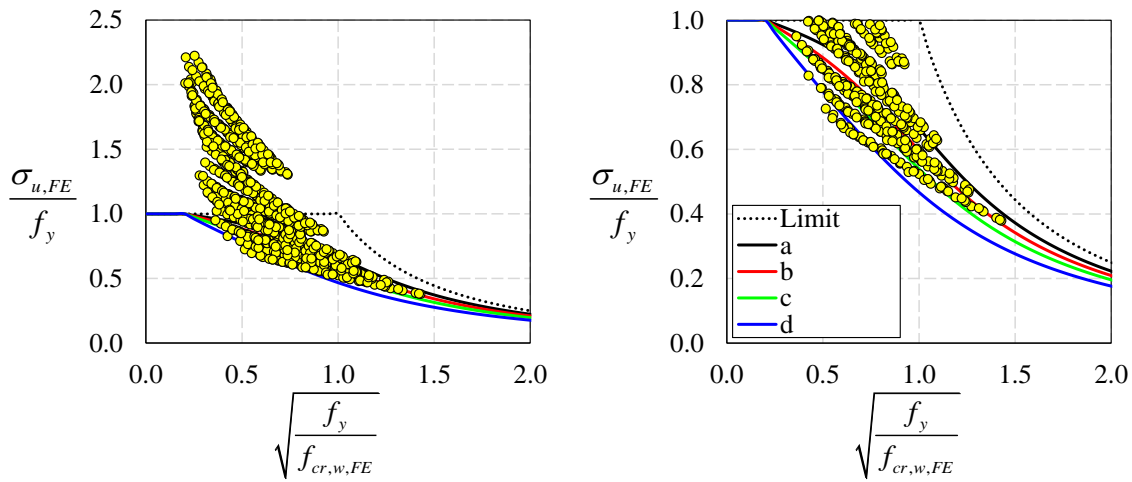
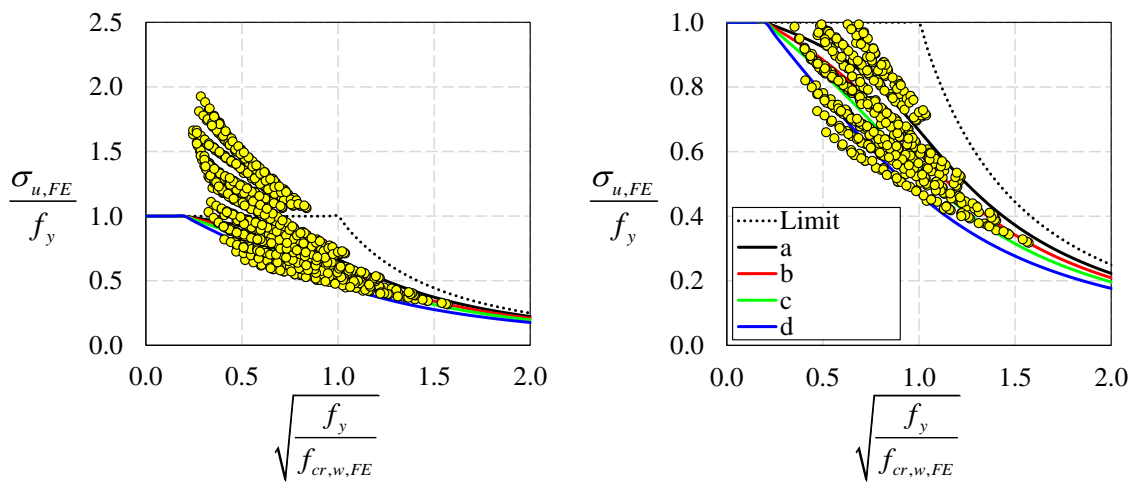
278

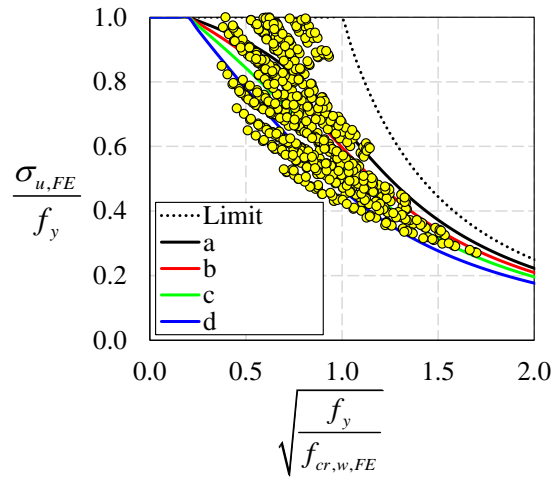
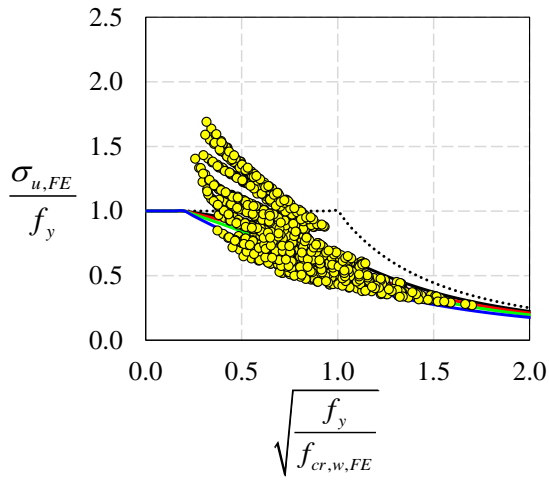
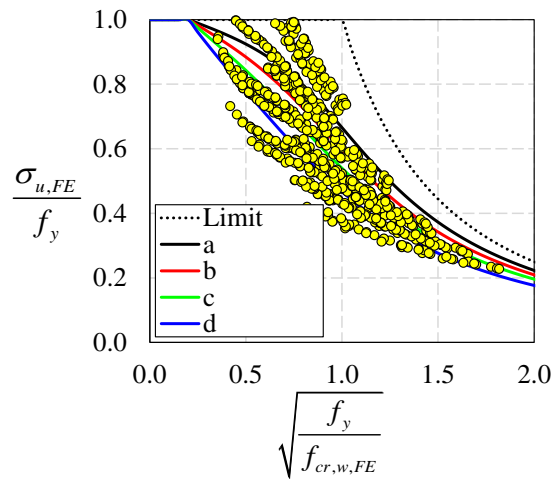
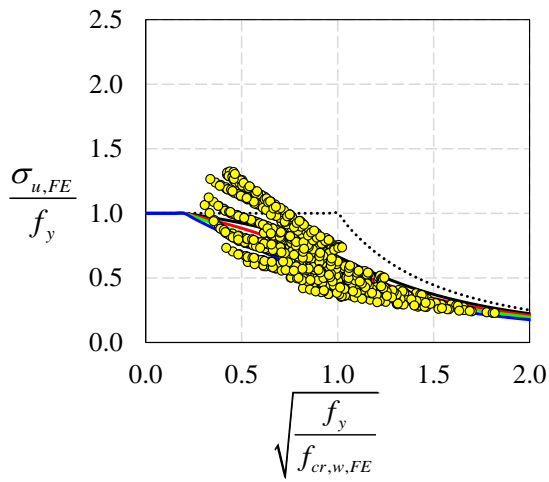
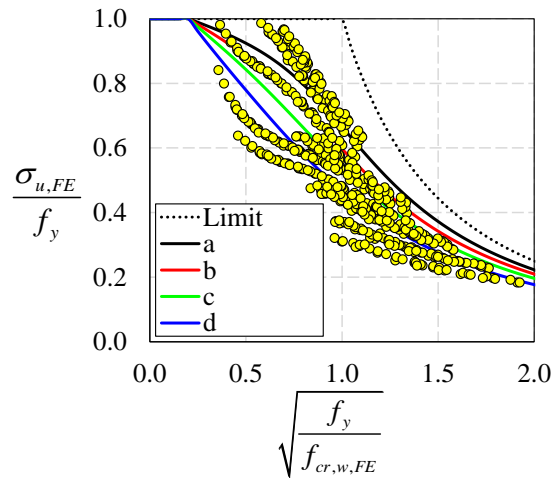
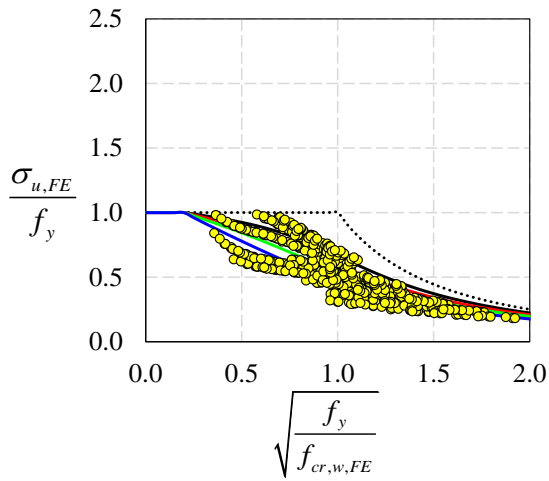
279 3.2 d_o/H ratio

280 **Fig. 8** shows the EC3 buckling curves in relation to the ratio of parameters that
 281 take into account the opening height variation to the final web height, after the
 282 castellation process. The results are illustrated considering $d_o/H=0.65$ (**Fig. 8a**),
 283 $d_o/H=0.70$ (**Fig. 8b**), $d_o/H=0.75$ (**Fig. 8c**), $d_o/H=0.80$ (**Fig. 8d**), $d_o/H=0.85$ (**Fig. 8e**) and
 284 $d_o/H=0.90$ (**Fig. 8f**). According to the results presented, it is possible to highlight that
 285 the lower the opening height, the greater the resistance. This can be explained in terms
 286 of the upper and lower tees sections, that is, the lower the height of the web opening is,
 287 the greater the height of the tee sections is, thus increasing the capacity to resist normal
 288 and tangential stresses.

289 Another point to be discussed refers to reduced slenderness (λ_o). For the range
 290 $0.65 \leq d_o/H \leq 0.80$ and considering $\lambda_o < 1.0$, it was verified that the maximum values of
 291 resistance exceeded the limit of resistance ($\sigma_{u,FE}/f_y > 1.0$), and the minimum values of
 292 resistance laid close to the buckling curve d . On the other hand, considering the ratio
 293 variation in $0.85 < d_o/H \leq 0.90$, there was a drop in capacity resistance. For these analysed
 294 models, it was verified that the maximum resistance values lie above the buckling curve

295 *a*, however, lower than the limit value ($1/\lambda_0^2$). Regarding the range of the ratio in
 296 $0.85 < d/H \leq 0.90$, it was observed that some models indicated resistance below the
 297 buckling curve *d* for values $\lambda_0 < 1.0$. This can be explained by the fact that their tee
 298 sections experienced instability phenomena before reaching the yield strength, for small
 299 values of applied loading.

(a) $d/H=0.65$ (b) $d/H=0.70$

(c) $d/dH=0.75$ (d) $d/dH=0.80$ (e) $d/dH=0.85$

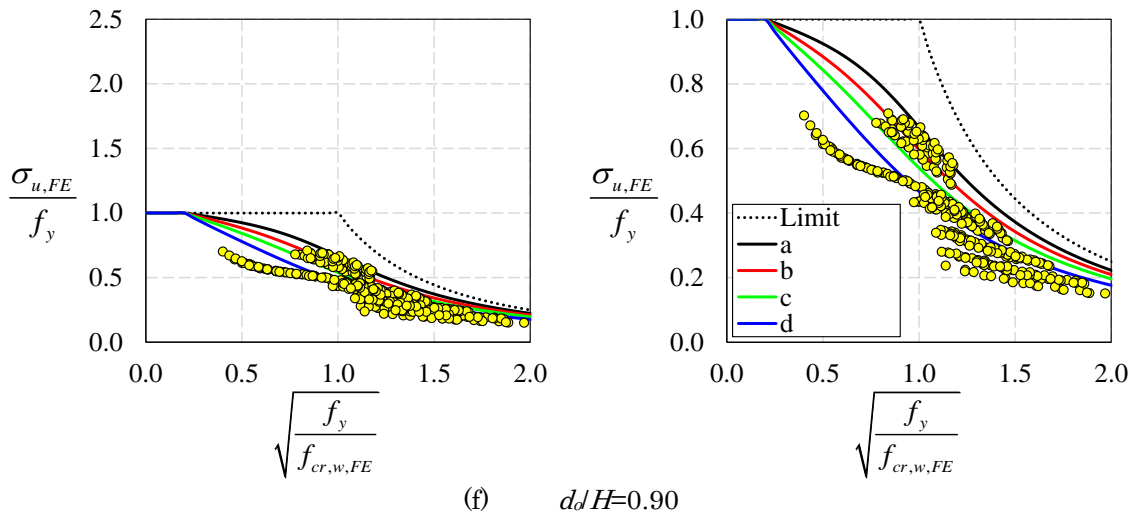


Fig. 8: d_o/H ratio vs. buckling curves of EC3

300

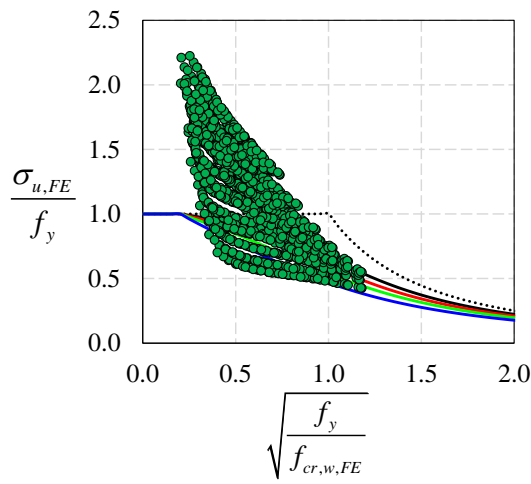
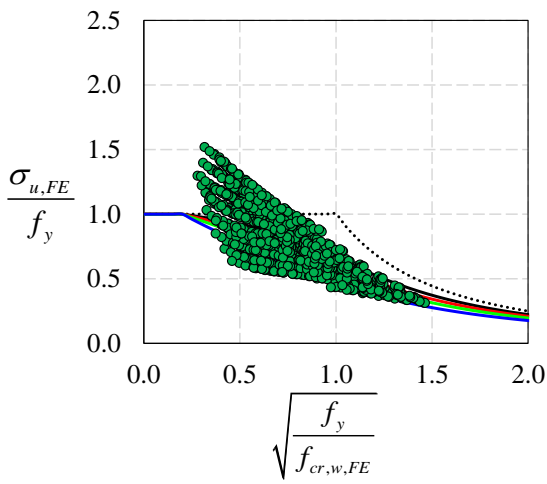
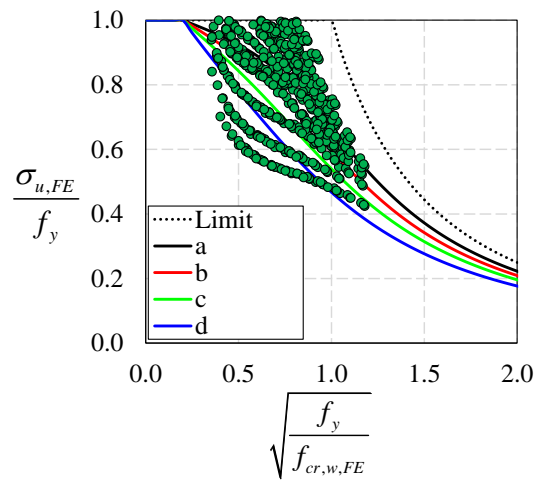
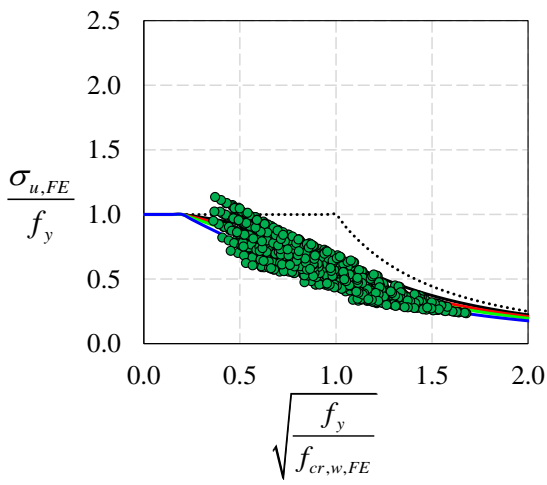
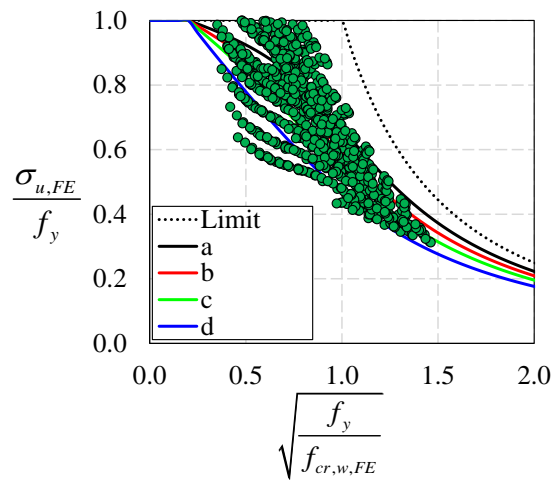
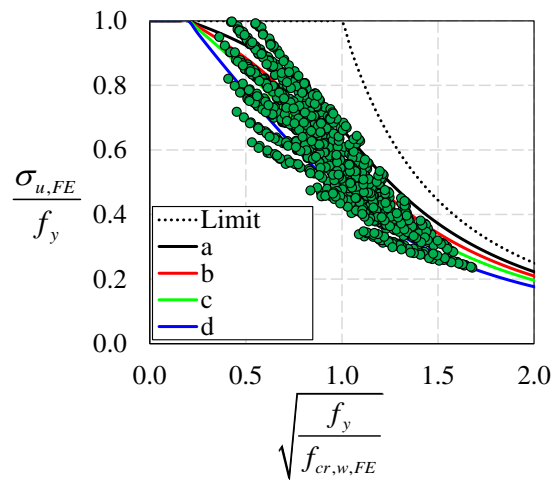
301

302 3.3 R/d_o ratio

303 The finite element results normalized with EC3 buckling curves and considered
 304 the ratio of the opening radius to opening height are shown in **Fig. 9**. It is important to
 305 note that the greater the opening radius, the greater the total height of the opening, as
 306 shown in **Fig. 1**. In this context, the results are presented considering $R/d_o=0.10$ (**Fig.**
 307 **9a**), $R/d_o=0.15$ (**Fig. 9b**), $R/d_o=0.20$ (**Fig. 9c**), $R/d_o=0.25$ (**Fig. 9d**) and $R/d_o=0.30$ (**Fig.**
 308 **9e**).

309 In this scenario, it is possible to highlight that as the opening radius increases,
 310 the resistance further decreases, showing that R/d_o is important in the resistance of
 311 steel beams with elliptically-based web openings. For $R/d_o=0.10-0.15$ and $\lambda_o < 1.0$, the
 312 maximum values of resistance exceeded the limit value, thus showing that the smaller
 313 the radius, the smaller the effective length. On the other hand, the minimum values of
 314 capacity resistance were found close to the buckling curve d . At last, for $R/d_o=0.20-0.30$
 315 and $0.5 \leq \lambda_o \leq 2.0$, there was a reduction between the maximum and minimum values of
 316 capacity resistance. In this scenario, most of the maximum resistance values were below
 317 the buckling curve a , and the minimum resistance values were below the buckling curve

318 *d.* These results presented here show that the web-post buckling resistance is sensitive
 319 to the parameter R/d_o .

(a) $R/d_o=0.10$ (b) $R/d_o=0.15$ (c) $R/d_o=0.20$ 

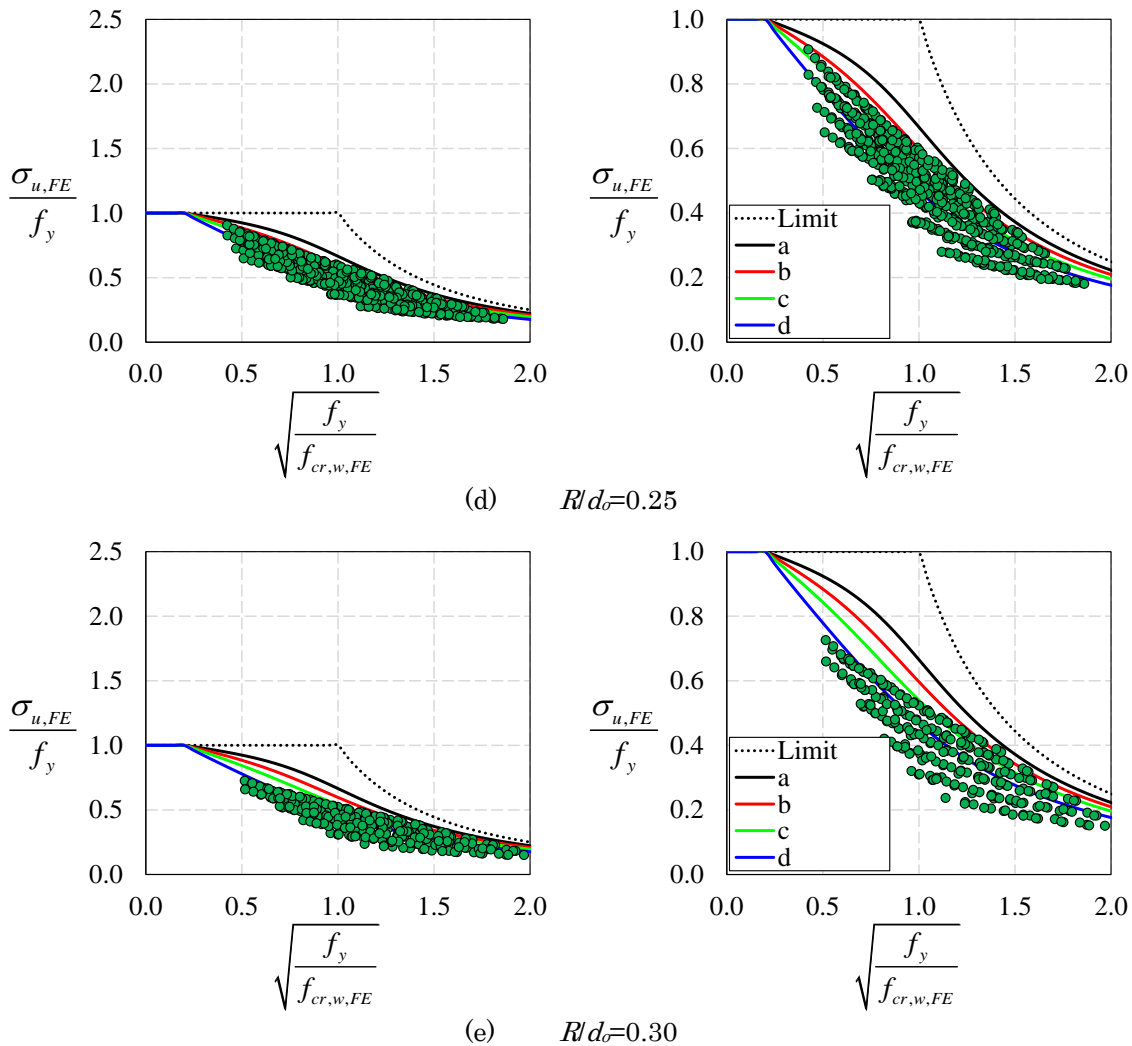


Fig. 9: R/d_o ratio vs. buckling curves of EC3

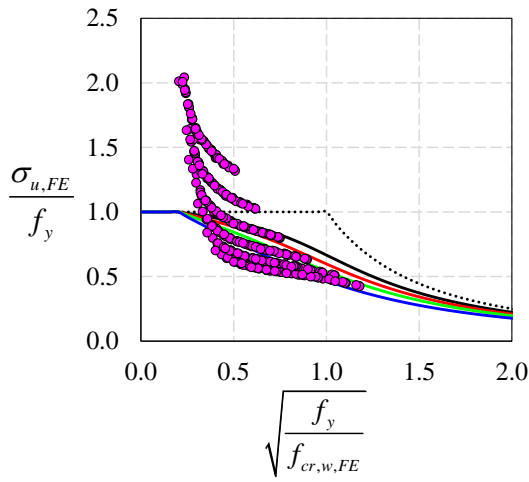
320

321

322 3.4 w/d_o ratio

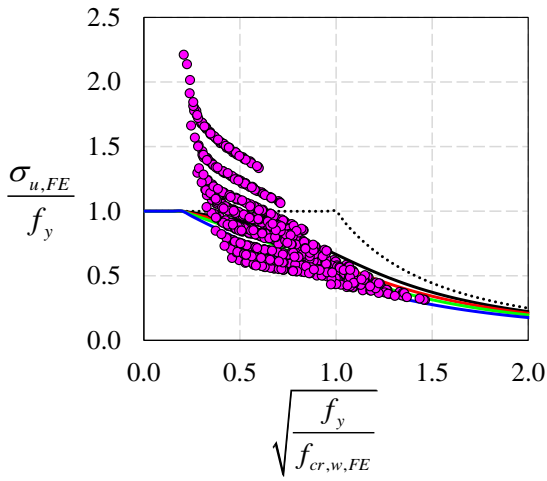
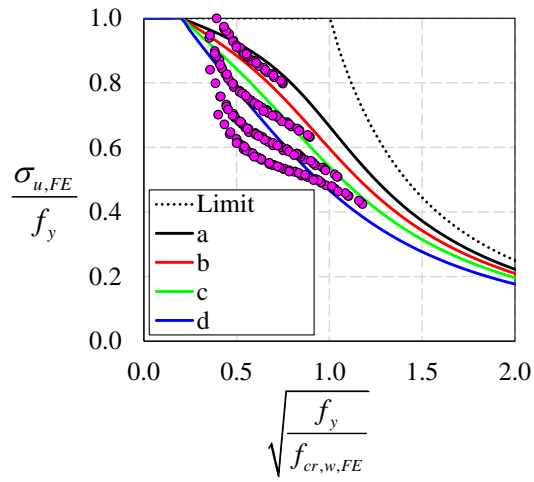
323 The parameter discussed herein represents the ratio between the width and
 324 height of the elliptically-based web opening (Fig 10). The ratios studied are $w/d_o=0.25$
 325 (Fig. 10a), $w/d_o=0.35$ (Fig. 10b), $w/d_o=0.45$ (Fig. 10c), $w/d_o=0.55$ (Fig. 10d) and $w/d_o=0.65$
 326 (Fig. 10e). For $\lambda_o < 1.0$, the maximum resistance values exceeded the limit, while the
 327 minimum resistance values remained close to the buckling curve d . Another observation
 328 that can be highlighted is that is that from $w/d_o=0.35$, the higher the w/d_o ratio, the
 329 greater the resistance. Fig. 11 illustrates two examples, considering the sections UB
 330 178x102x19 (Fig. 11a) and UB 1016x305x487 (Fig 11b). Although the H/d , d_o/H and R/d_o

331 ratios were kept constant for the analysis, the resistance variation as a function of the
 332 w/d_o proved to be more sensitive for the UB 1016x305x487, which has a thicker web.



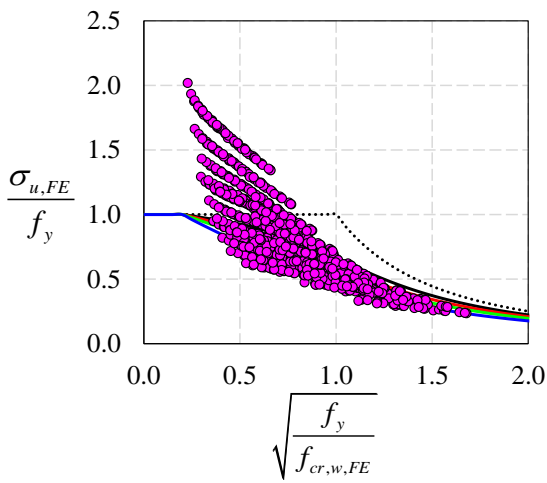
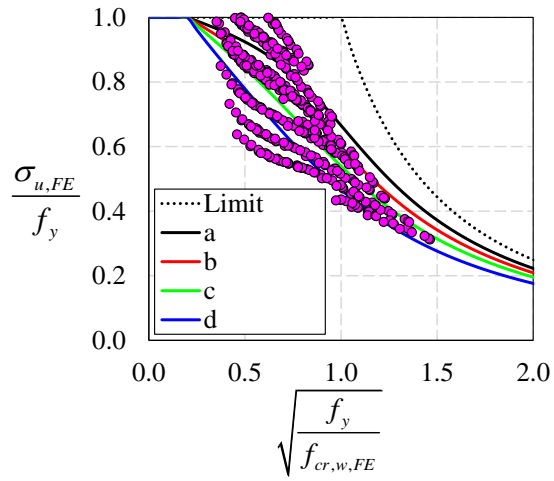
(a)

$w/d_o=0.25$



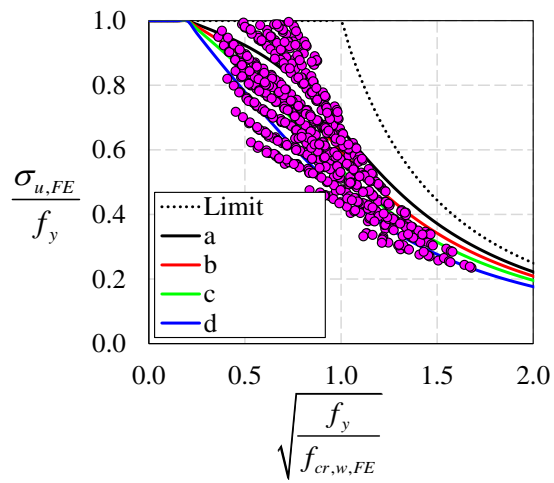
(b)

$w/d_o=0.35$



(c)

$w/d_o=0.45$



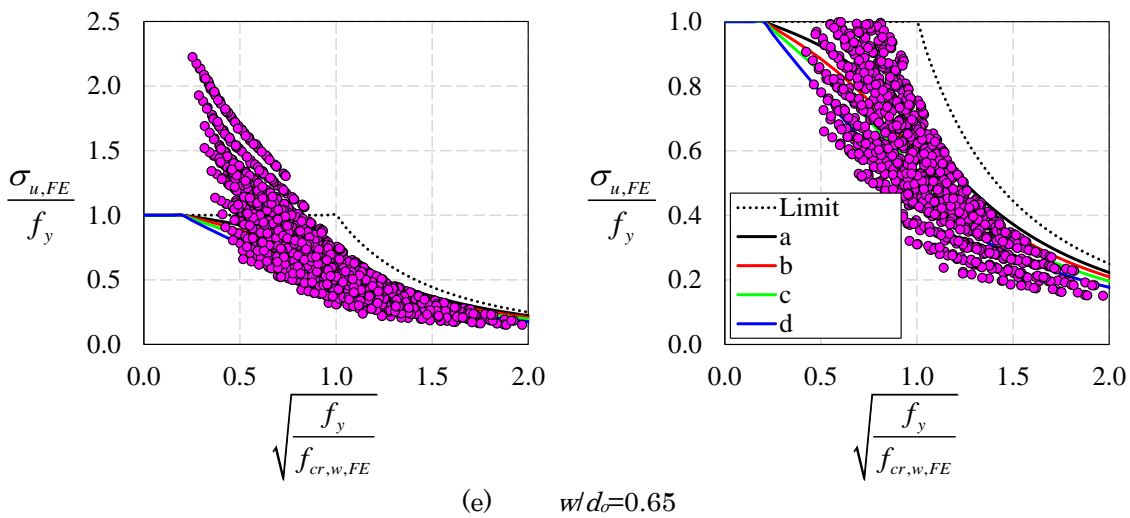
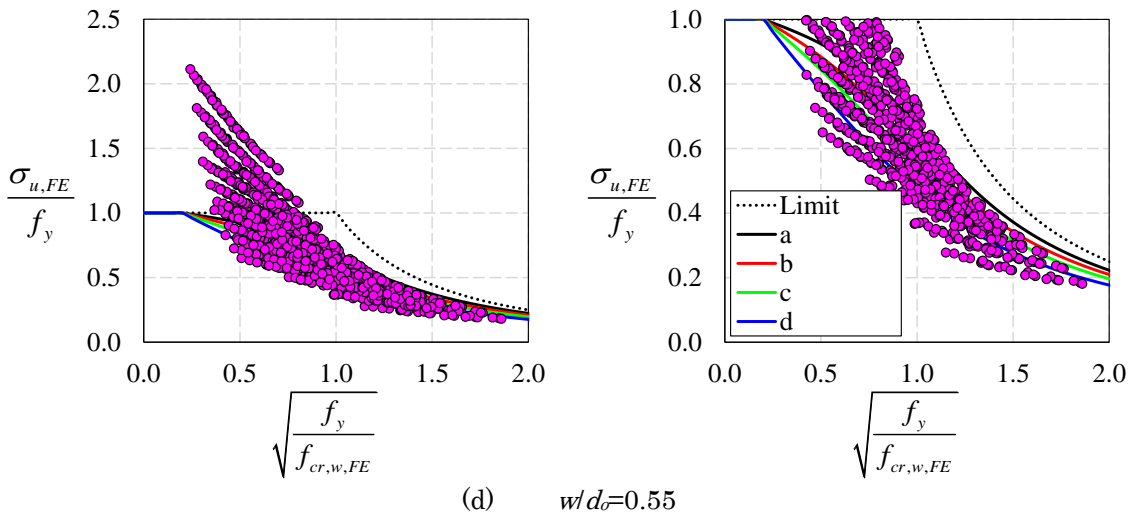
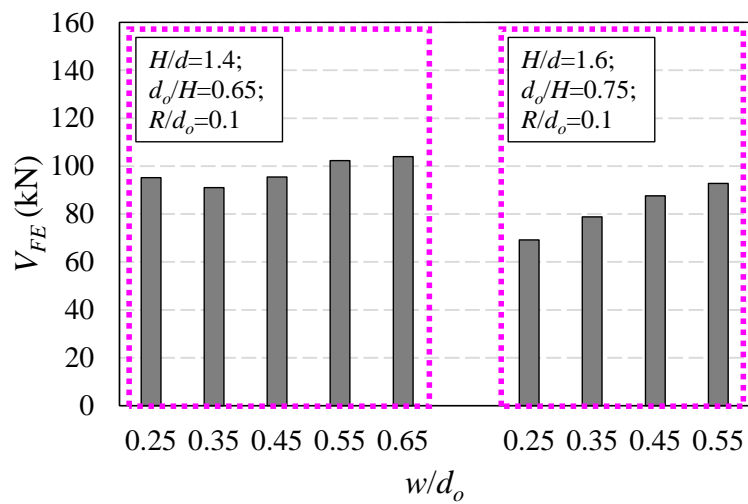


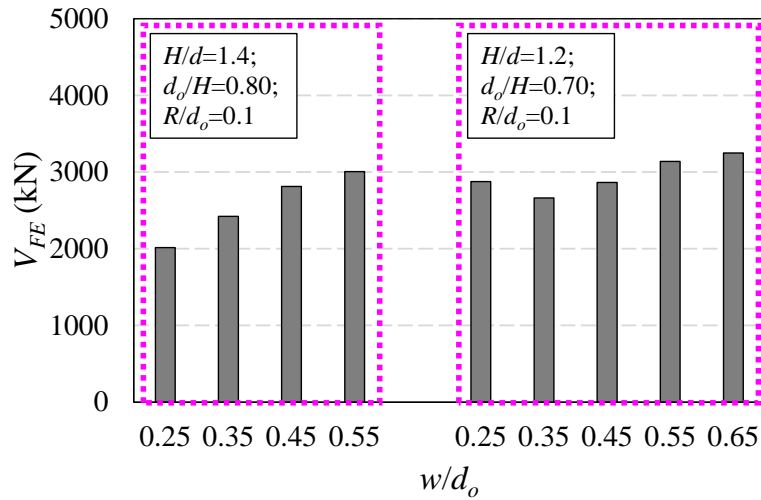
Fig. 10: w/d_0 ratio vs. buckling curves of EC3

333

334



(a) UB 178x102x19



(b) UB 1016x305x487

Fig. 11: Influence of w/d_o on web-post buckling resistance.

335

336 4. DESIGN APPROACH

337 An approach for calculating the web-post buckling resistance of steel beams with
 338 elliptically-based web openings is presented. The hypothesis that the buckling occurs
 339 within a flexible region, which is delimited by the red dashed lines in the **Fig. 12**. The
 340 compressed strut is then defined as seen in the same figure. This is a methodology
 341 similar to the one presented in SCI P355 [17], however, effective length of the strut that
 342 considers the geometric parameters of the elliptically-based web openings is derived.
 343 The numerical effective length from the parametric study is estimated from the critical
 344 shear stress acting in the web-post using **Eq. (9)**, then the web-post slenderness is
 345 calculated using **Eq. (11)**. Once the web-post slenderness has been determined, the
 346 effective length is estimated using **Eq. (12)**.

$$\lambda_{w,FE} = \sqrt{\frac{\pi^2 E}{f_{cr,w,FE}}} = \sqrt{\frac{\pi^2 E}{\frac{V_{cr,FE}}{t_w (s-w)}}} \quad (11)$$

$$l_{eff,FE} = \frac{\lambda_{w,FE} t_w}{\sqrt{12}} \quad (12)$$

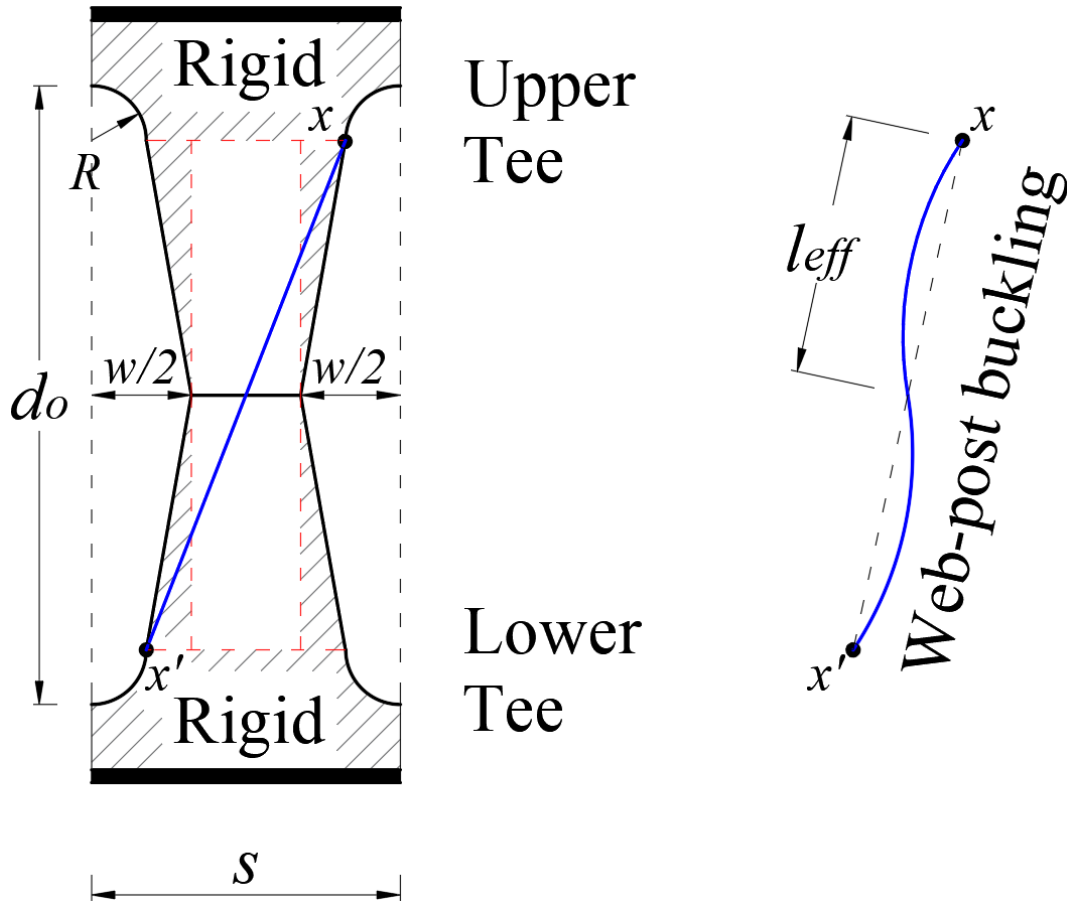


Fig. 12: Approach to effective web-post length (l_{eff})

347

348

349

350

351

352

353

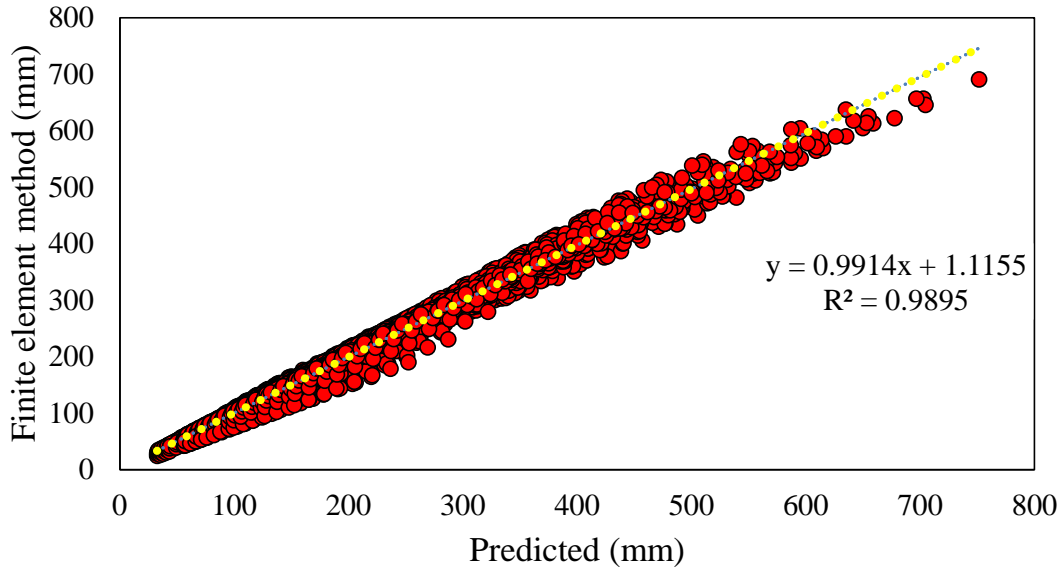
354

To define the effective length, a calibration process with the numerical results is required. The effective length would be a function of the cellular beam geometry as well as the tee sections that restrain the buckling of the strut. Once the effective length limit value is determined from the FE results, an approximation of this value is calculated (Eqs. 13-14) as a function of the hypothesis presented in Fig. 12, in which k is an adjustment factor determined by the linear regression of the studied parameters.

$$l_{eff} = k \sqrt{\left(\frac{d_o - 2R}{2}\right)^2 + \left(\frac{s}{2} - R\right)^2} \quad (13)$$

$$k = 0.516 - 0.288 \left(\frac{H}{d_o}\right) + 0.062 \left(\frac{s}{s-w}\right) + 2.384 \left(\frac{s}{d_o}\right) - 2.906 \left(\frac{w}{d_o}\right) \quad (14)$$

355 In **Fig. 13** the comparison between the values of the effective lengths is presented.
 356 **Table 5** shows the statistical analysis of the results for the calculation of the effective
 357 length.



358

359 **Fig. 13: Effective length – finite element method vs. predicted**

359

360 **Table 5: Statistical analysis for effective length prediction**

Analysis	Value
R ² (Regression)	0.9895
RMSE (Root Mean Square Error) (mm)	11.991
MAE (Mean Absolute Error) (mm)	7.954
Minimum relative error	-9.70%
Maximum relative error	34.22%
Average (FEM/Predicted)	0.996
S.D.	5.67%
Var.	0.32%

361 Once the web-post effective length of perforated steel beams with elliptically-
 362 based web openings is determined (**Eqs. 13-14**), the procedure for calculating the web-
 363 post buckling resistance, V_{Rk} can be followed, according to **Eqs. (15-22)**, using the
 364 buckling curve c as shown in **Table 4**:

$$\lambda_w = \frac{l_{eff} \sqrt{12}}{t_w} \quad (15)$$

$$f_{cr,w} = \frac{\pi^2 E}{\lambda_w^2} \quad (16)$$

$$\lambda_0 = \sqrt{\frac{f_y}{f_{cr,w}}} \quad (17)$$

$$\phi = 0.5 \left[1 + 0.49 (\lambda_0 - 0.2) + \lambda_0^2 \right] \quad (18)$$

$$\chi = \frac{1}{\phi + \sqrt{\phi^2 - \lambda_0^2}} \leq 1.0 \quad (19)$$

$$\sigma_{Rk} = K \chi f_y \quad (20)$$

$$K = -1.318 + 1.790 \left(\frac{H}{d_o} \right) + 0.413 \left(\frac{s}{s-w} \right) - 1.926 \left(\frac{s}{d_o} \right) + 0.937 \left(\frac{w}{d_o} \right) - 0.02 \left(\frac{d_o}{t_w} \right) + 1.412 \lambda_0 \quad (21)$$

$$V_{Rk} = \sigma_{Rk} t_w (s-w) \quad (22)$$

365 In the next section, the design approach is compared with 4,344 models developed
366 in the parametric study.

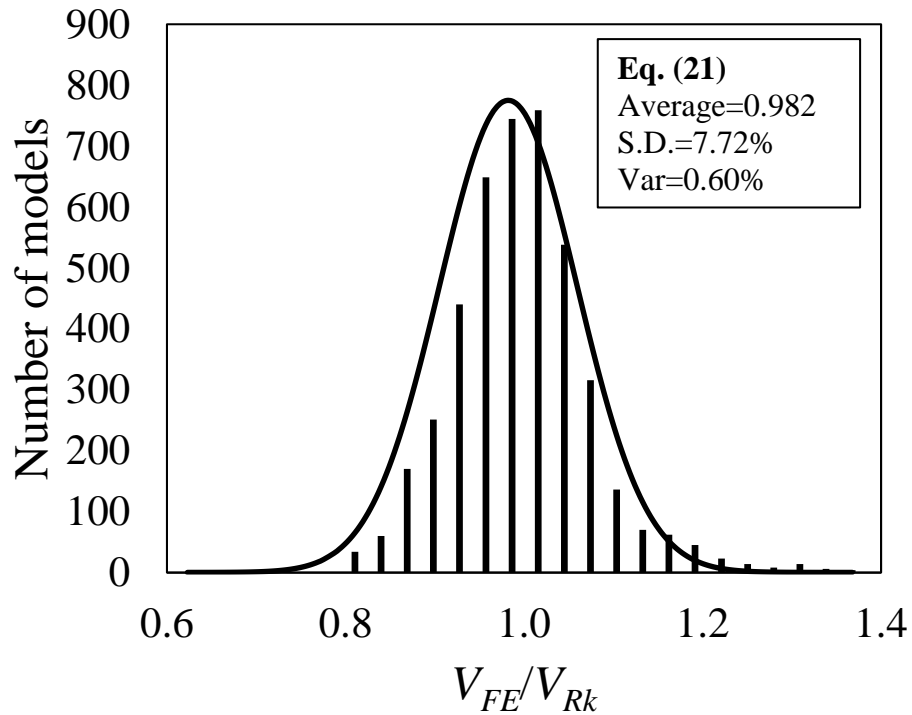
367

368 5. VERIFICATION

369 As previously described, in this section the accuracy of the proposed method is
370 verified with the finite element method results. **Fig 14** and **Fig 15** show the normal
371 distribution and the regression analyses, respectively, considering 4,344 models. It is
372 predicted that the mean, standard deviation and variance were 0.982, 7.72% and 0.60%,
373 respectively. The maximum and minimum relative errors between finite element
374 analyses and **Eq. (21)** were -26.89% and 28.02%, respectively. **Table 6** presents the

375 summary of the statistical analysis, also considering the Root Mean Square Error
 376 (RMSE) and the Mean Absolute Error (MAE).

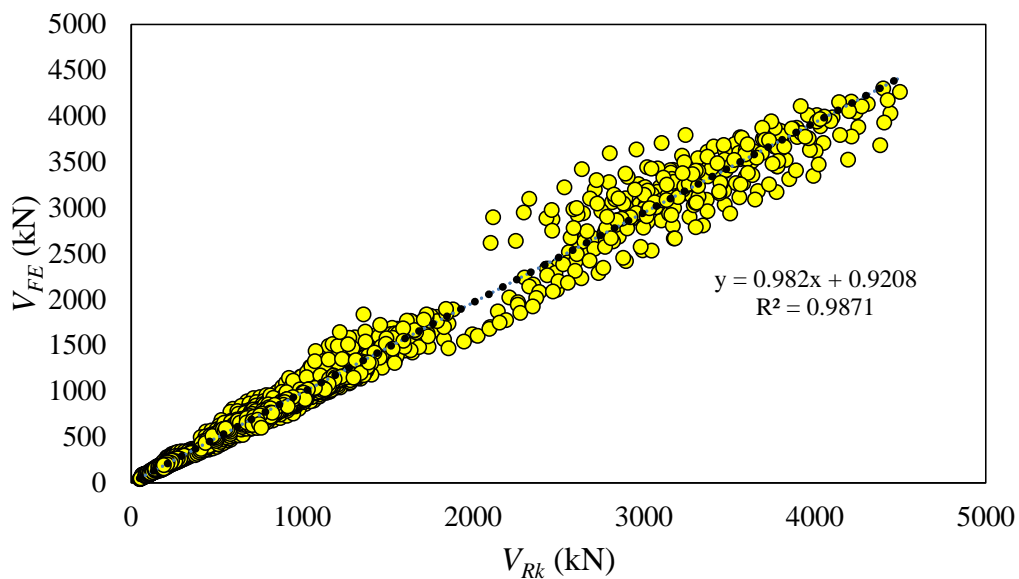
377 It is evident that the proposed novel design equation seems to predict WPB shear
 378 capacity of elliptically-based cellular beam results that are in reasonable agreement
 379 with the finite element results.



380

381

Fig. 14: Normal distribution – Finite element analyses vs. Design Approach



382

383

Fig. 15: Web-post buckling resistance – finite element method vs. predicted

384 **Table 6: Statistical analysis for web-post buckling calculation procedure**

Analysis	Value
R ² (Regression)	0.9871
RMSE (Root Mean Square Error) (kN)	91.09
MAE (Mean Absolute Error) (kN)	46.24
Minimum relative error	-26.89%
Maximum relative error	28.02%
Average (FEM/Predicted)	0.982
S.D.	7.71%
Var.	0.59%

385

386 **6. A STATISTICAL EVALUATION IN THE FASHION OF ANNEX D EN 1990**

387 A statistical analysis following the provisions of Annex D EN 1990 [37] has been
388 carried out in order to assess the reliability of the proposed design method. **Table 7**
389 illustrates the key statistical parameters, including the number of tests and finite
390 element data n , the design fractile factor (ultimate limit state) $k_{d,n}$, the average ratio of
391 FE to model resistance based on a least squares fit to all the data \bar{b} , the combined
392 coefficient of variation incorporating both model and basic variable uncertainties V_r and
393 the partial safety factor for cross section resistance γ_{M0} . The material over-strength of
394 high strength steel was taken equal to 1.25 with a coefficient of variation COV of 0.055
395 [35]. The COV between the experimental and the numerical results, which was found
396 0.0133, is also considered. The COV for the geometric properties is taken as 0.028.
397 Performing a First Order Reliability Method (FORM) in accordance with the Eurocode
398 target reliability requirements, the partial factor γ_{M0} is 0.96. As the partial factor is
399 close to unity, the value of $\gamma_{M0}=1.00$ as recommended in EC3 [18], is appropriate for the
400 design of steel beams with elliptically-based web openings in WPB.

401

402 **Table 7: Summary of the reliability analysis for the proposed method**

n	\bar{b}	$k_{d,n}$	V_r	γ_{M0}
4344	0.982	3.04	0.1	0.96

403

404 **CONCLUDING REMARKS**

405 The present work studies the web-post buckling resistance of perforated steel
406 beams with elliptically-based web openings. A finite element method was developed
407 based on tests from the literature, considering full and single web-post models. A
408 parametric study was carried out using Python to automate data processing. Post-
409 buckling analysis was conducted by geometrically and materially nonlinear analysis
410 with imperfections. From 5,400 geometric models, 4,344 had the failure mode
411 characterized by the WPB. The results were used to propose a design approach for the
412 buckling resistance of the strut model analogy, in which the compressive stress was
413 calculated using EC3 approach. The effective length of elastic buckling was defined and
414 properly calibrated by regression, and the web-post buckling resistance is calculated
415 using the buckling curve c. It was concluded:

- 416 i. The smaller the expansion factor (H/d), the smaller the web-post slenderness (λ_w),
417 and consequently, the smaller the effective length (l_{eff}). This causes an increase
418 in capacity resistance.
- 419 ii. The lower the height of the elliptically-based web opening (d_o), the greater the
420 capacity resistance. This can be explained in terms of the upper and lower tee
421 sections, that is, the lower the height of the web opening, the greater the height
422 of the tee sections (d_t and d_b), thus increasing the capacity to resist normal and
423 tangential stresses.

- 424 iii. As the opening radius (R/d_o) increases, the resistance further decreases, showing
 425 that ratio is important in the resistance of steel beams with elliptically-based web
 426 openings.
- 427 iv. The resistance showed sensitivity as a function of w/d_o ratio. However, this
 428 sensitivity can be more significant with the variation of geometric parameters of
 429 the section, such as web.
- 430 v. The proposed analytical model for the WPB resistance was verified by a reliability
 431 analysis and confirmed that it is appropriate for the design of perforated steel
 432 beams with elliptically-based web openings.

433

434 **REFERENCES**

- 435 [1] ArcelorMittal. ACB® and Angelina® beams - A New Generation of Cellular Beams
 436 2018.
- 437 [2] Ferreira FPV, Shamass R, Limbachiya V, Tsavdaridis KD, Martins CH. Lateral-
 438 torsional buckling resistance prediction model for steel cellular beams generated
 439 by Artificial Neural Networks (ANN). *Thin-Walled Struct* 2022;170:108592.
 440 <https://doi.org/10.1016/j.tws.2021.108592>.
- 441 [3] Ellobody E. Nonlinear analysis of cellular steel beams under combined buckling
 442 modes. *Thin-Walled Struct* 2012;52:66–79.
 443 <https://doi.org/10.1016/j.tws.2011.12.009>.
- 444 [4] Panedpojaman P, Sae-Long W, Chub-Uppakarn T. Cellular beam design for
 445 resistance to inelastic lateral-torsional buckling. *Thin-Walled Struct*
 446 2016;99:182–94. <https://doi.org/10.1016/j.tws.2015.08.026>.
- 447 [5] Ellobody E. Interaction of buckling modes in castellated steel beams. *J Constr*
 448 *Steel Res* 2011;67:814–25. <https://doi.org/10.1016/j.jcsr.2010.12.012>.
- 449 [6] Weidlich CM, Sotelino ED, Cardoso DCT. An application of the direct strength
 450 method to the design of castellated beams subject to flexure. *Eng Struct*
 451 2021;243:112646. <https://doi.org/10.1016/j.engstruct.2021.112646>.
- 452 [7] Ferreira FPV, Martins CH. LRFD for Lateral-Torsional Buckling Resistance of
 453 Cellular Beams. *Int J Civ Eng* 2020;18:303–23. <https://doi.org/10.1007/s40999-019-00474-7>.
- 454
- 455 [8] Morkhade SG, Gupta LM. Experimental investigation for failure analysis of steel
 456 beams with web openings. *Steel Compos Struct* 2017;23:647–56.
 457 <https://doi.org/10.12989/SCS.2017.23.6.647>.

- 458 [9] Kerdal D, Nethercot DA. Failure modes for castellated beams. *J Constr Steel Res*
459 1984;4:295–315. [https://doi.org/10.1016/0143-974X\(84\)90004-X](https://doi.org/10.1016/0143-974X(84)90004-X).
- 460 [10] Grilo LF, Fakury RH, Castro e Silva ALR de, Veríssimo G de S. Design procedure
461 for the web-post buckling of steel cellular beams. *J Constr Steel Res* 2018;148:525–
462 41. <https://doi.org/10.1016/j.jcsr.2018.06.020>.
- 463 [11] Tsavdaridis KD, D’Mello C. Web buckling study of the behaviour and strength of
464 perforated steel beams with different novel web opening shapes. *J Constr Steel*
465 *Res* 2011;67:1605–20. <https://doi.org/10.1016/j.jcsr.2011.04.004>.
- 466 [12] Limbachiya V, Shamass R. Application of Artificial Neural Networks for web-post
467 shear resistance of cellular steel beams. *Thin-Walled Struct* 2021;161:107414.
468 <https://doi.org/10.1016/j.tws.2020.107414>.
- 469 [13] Panedpojaman P, Thepchatri T, Limkatanyu S. Novel design equations for shear
470 strength of local web-post buckling in cellular beams. *Thin-Walled Struct*
471 2014;76:92–104. <https://doi.org/10.1016/j.tws.2013.11.007>.
- 472 [14] Fares SS, Coulson J, Dinehart DW. *AISC Steel Design Guide 31: Castellated and*
473 *Cellular Beam Design*. American Institute of Steel Construction; 2016.
- 474 [15] American Institute of Steel Construction. *ANSI/AISC 360-16 - Specification for*
475 *structural steel buildings*. 2016.
- 476 [16] Ward JK. *Design of Composite and Non-Composite Cellular Beams*. Silwood Park,
477 Ascot, UK: Steel Construction Institute; 1990.
- 478 [17] Lawson RM, Hicks SJ. *Design of composite beams with large web openings*. SCI
479 P355. The Steel Construction Institute; 2011.
- 480 [18] European committee for standardization. *EN 1993-1-1: Eurocode 3 – Design of*
481 *steel structures – Part 1-1: General rules and rules for buildings* 2002.
- 482 [19] Tsavdaridis KD, D’Mello C. FE Investigation of Perforated Sections with Standard
483 and Non-Standard Web Opening Configurations and Sizes. In: Chan SL, editor.
484 6th Int. Conf. Adv. in Steel Struct., Hong Kong, China: Hong Kong Institute of
485 Steel Construction; 2009, p. 213–20.
- 486 [20] Tsavdaridis KD. *Structural performance of perforated steel beams with novel web*
487 *openings and with partial concrete encasement*. City University London; 2010.
- 488 [21] Tsavdaridis KD, Kingman JJ, Toropov V V. Application of structural topology
489 optimisation to perforated steel beams. *Comput Struct* 2015;158:108–23.
490 <https://doi.org/10.1016/j.compstruc.2015.05.004>.
- 491 [22] Tsavdaridis KD, D’Mello C. Vierendeel Bending Study of Perforated Steel Beams
492 with Various Novel Web Opening Shapes through Nonlinear Finite-Element
493 Analyses. *J Struct Eng* 2012;138:1214–30. [https://doi.org/10.1061/\(asce\)st.1943-541x.0000562](https://doi.org/10.1061/(asce)st.1943-541x.0000562).
- 494
- 495 [23] Tsavdaridis KD, D’Mello C. Optimisation of novel elliptically-based web opening
496 shapes of perforated steel beams. *J Constr Steel Res* 2012;76:39–53.
497 <https://doi.org/10.1016/j.jcsr.2012.03.026>.

- 498 [24] Tsavdaridis KD, D’Mello C. Structural beam. GB 2492176, 2012.
- 499 [25] Zaarour W, Redwood R. Web Buckling in Thin Webbed Castellated Beams. *J*
500 *Struct Eng* 1996;122:860–6. [https://doi.org/10.1061/\(ASCE\)0733-](https://doi.org/10.1061/(ASCE)0733-9445(1996)122:8(860))
501 9445(1996)122:8(860).
- 502 [26] Tsavdaridis KD, Galiatsatos G. Assessment of cellular beams with transverse
503 stiffeners and closely spaced web openings. *Thin-Walled Struct* 2015;94:636–50.
504 <https://doi.org/10.1016/j.tws.2015.05.005>.
- 505 [27] Durif S, Bouchaïr A, Vassart O. Experimental and numerical investigation on
506 web-post specimen from cellular beams with sinusoidal openings. *Eng Struct*
507 2014;59:587–98. <https://doi.org/10.1016/j.engstruct.2013.11.021>.
- 508 [28] Ferreira FPV, Tsavdaridis KD, Martins CH, De Nardin S. Buckling and post-
509 buckling analyses of composite cellular beams. *Compos Struct* 2021;262.
510 <https://doi.org/10.1016/j.compstruct.2021.113616>.
- 511 [29] Ferreira FPV, Martins CH, De Nardin S. Sensitivity Analysis of Composite
512 Cellular Beams to Constitutive Material Models and Concrete Fracture. *Int J*
513 *Struct Stab Dyn* 2021;21:2150008. <https://doi.org/10.1142/S0219455421500085>.
- 514 [30] Ferreira FPV, Tsavdaridis KD, Martins CH, De Nardin S. Ultimate strength
515 prediction of steel–concrete composite cellular beams with PCHCS. *Eng Struct*
516 2021;236:112082. <https://doi.org/10.1016/j.engstruct.2021.112082>.
- 517 [31] Ferreira FPV, Rossi A, Martins CH. Lateral-torsional buckling of cellular beams
518 according to the possible updating of EC3. *J Constr Steel Res* 2019;153:222–42.
519 <https://doi.org/10.1016/j.jcsr.2018.10.011>.
- 520 [32] Ferreira FPV, Martins CH, De Nardin S. Assessment of web post buckling
521 resistance in steel-concrete composite cellular beams. *Thin-Walled Struct*
522 2021;158:106969. <https://doi.org/10.1016/j.tws.2020.106969>.
- 523 [33] Ferreira FPV, Tsavdaridis KD, Martins CH, De Nardin S. Composite action on
524 web-post buckling shear resistance of composite cellular beams with PCHCS and
525 PCHCSCT. *Eng Struct* 2021;246:113065.
526 <https://doi.org/10.1016/j.engstruct.2021.113065>.
- 527 [34] Rajana K, Tsavdaridis KD, Koltsakis E. Elastic and inelastic buckling of steel
528 cellular beams under strong-axis bending. *Thin-Walled Struct* 2020;156:106955.
529 <https://doi.org/10.1016/j.tws.2020.106955>.
- 530 [35] Shamass R, Guarracino F. Numerical and analytical analyses of high-strength
531 steel cellular beams: A discerning approach. *J Constr Steel Res* 2020;166:105911.
532 <https://doi.org/10.1016/j.jcsr.2019.105911>.
- 533 [36] Yun X, Gardner L. Stress-strain curves for hot-rolled steels. *J Constr Steel Res*
534 2017;133:36–46. <https://doi.org/10.1016/j.jcsr.2017.01.024>.
- 535 [37] European committee for standardization. EN 1990: Eurocode – Basis of structural
536 design n.d.